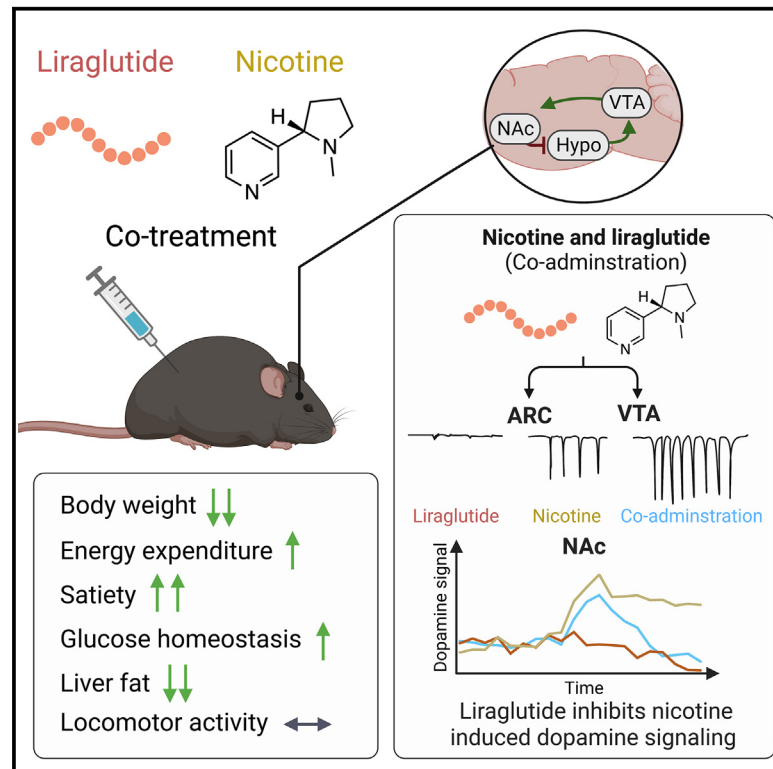


# GLP-1 and nicotine combination therapy engages hypothalamic and mesolimbic pathways to reverse obesity

## Graphical abstract



## Authors

Sarah Falk, Jonas Petersen, Charlotte Svendsen, ..., Ulrik Gether, Kristi A. Kohlmeier, Christoffer Clemmensen

## Correspondence

chc@sund.ku.dk

## In brief

Falk et al. demonstrate that nicotine potentiates GLP-1 receptor agonist-driven weight loss in obese mice. Co-administration of nicotine and liraglutide triggers neuronal activity in the hypothalamus, brainstem, and mesolimbic reward system, leading to increased energy expenditure and decreased food intake. Liraglutide attenuates nicotine-induced dopamine release in the nucleus accumbens.

## Highlights

- Nicotine and liraglutide synergistically lower body weight in obese mice
- Nicotine and liraglutide reduce food intake and increase energy expenditure
- There is cross-sensitization between GLP-1R and nAChR in the ARC and VTA
- Liraglutide diminishes nicotine-induced dopamine signaling in the accumbens



## Article

# GLP-1 and nicotine combination therapy engages hypothalamic and mesolimbic pathways to reverse obesity

Sarah Falk,<sup>1</sup> Jonas Petersen,<sup>1,2</sup> Charlotte Svendsen,<sup>1</sup> Cesar R. Romero-Leguizamón,<sup>2</sup> Søren Heide Jørgensen,<sup>3</sup> Nathalie Krauth,<sup>1,3</sup> Mette Q. Ludwig,<sup>1</sup> Kathrine Lundø,<sup>1</sup> Urmas Roostalu,<sup>4</sup> Grethe Skovbjerg,<sup>1,4</sup> Duy Anh Gurskov Nielsen,<sup>1</sup> Aske Lykke Ejdrup,<sup>3</sup> Tune H. Pers,<sup>1</sup> Oksana Dmytriyeva,<sup>1</sup> Jacob Hecksher-Sørensen,<sup>4</sup> Ulrik Gether,<sup>3</sup> Kristi A. Kohlmeier,<sup>2</sup> and Christoffer Clemmensen<sup>1,5,\*</sup>

<sup>1</sup>Novo Nordisk Foundation Center for Basic Metabolic Research, Faculty of Health and Medical Sciences, University of Copenhagen, Copenhagen, Denmark

<sup>2</sup>Department of Drug Design and Pharmacology, Faculty of Health and Medical Sciences, University of Copenhagen, Copenhagen, Denmark

<sup>3</sup>Department of Neuroscience, Faculty of Health and Medical Sciences, University of Copenhagen, Copenhagen, Denmark

<sup>4</sup>Gubra, Hørsholm, Denmark

<sup>5</sup>Lead contact

\*Correspondence: [chc@sund.ku.dk](mailto:chc@sund.ku.dk)

<https://doi.org/10.1016/j.celrep.2023.112466>

## SUMMARY

Glucagon-like peptide-1 receptor (GLP-1R) agonists promote nicotine avoidance. Here, we show that the crosstalk between GLP-1 and nicotine extends beyond effects on nicotine self-administration and can be exploited pharmacologically to amplify the anti-obesity effects of both signals. Accordingly, combined treatment with nicotine and the GLP-1R agonist, liraglutide, inhibits food intake and increases energy expenditure to lower body weight in obese mice. Co-treatment with nicotine and liraglutide gives rise to neuronal activity in multiple brain regions, and we demonstrate that GLP-1R agonism increases excitability of hypothalamic proopiomelanocortin (POMC) neurons and dopaminergic neurons in the ventral tegmental area (VTA). Further, using a genetically encoded dopamine sensor, we reveal that liraglutide suppresses nicotine-induced dopamine release in the nucleus accumbens in freely behaving mice. These data support the pursuit of GLP-1R-based therapies for nicotine dependence and encourage further evaluation of combined treatment with GLP-1R agonists and nicotinic receptor agonists for weight loss.

## INTRODUCTION

The prevalence of obesity has nearly tripled since 1975, and obesity is now estimated to affect more than 764 million individuals globally.<sup>1</sup> Excess body fat increases the risk of several non-communicable diseases, including type 2 diabetes and cardiovascular disease, and is associated with decreased life expectancy.<sup>2–4</sup> Recent progress in anti-obesity drug development has pioneered a series of effective anti-obesity medicines based on pharmacokinetically optimized gut peptide hormones, delivering 15%–20% weight loss in human subjects with obesity.<sup>5,6</sup> However, dose-dependent gastrointestinal adverse events limit the maximal efficacy that can be achieved with the current glucagon-like peptide-1 (GLP-1)-based therapies, and combinatorial treatment approaches are likely required to amplify weight loss efficacy without compromising safety.<sup>7–10</sup> Smoking affects energy balance, and the prospect of weight gain is reported to discourage smoking cessation.<sup>11</sup> Nicotine is the principal component underlying the effects of smoking on energy

balance,<sup>12</sup> and nicotine reduces appetite and increases energy expenditure via activating central and peripheral nicotinic acetylcholine receptors (nAChRs).<sup>12</sup> Pharmacological stimulation of neuronal nAChRs affects both homeostatic feeding pathways and circuits involved in food reward,<sup>13–16</sup> and both central and peripheral nAChRs promote adipose tissue thermogenesis.<sup>14,17,18</sup> Despite the pleiotropic effects of nAChR agonism on energy balance and feeding behavior, the potential therapeutic virtues of nicotine analogs for treatment of metabolic diseases have received relatively little attention, likely because of nicotine's infamous role in tobacco addiction. GLP-1R activation enhances nicotine-induced neuronal excitability and diminishes nicotine self-administration in rodent models.<sup>19</sup> This observation raises the possibility that GLP-1R activation might act as a universal sensitizer of nicotine pharmacology, including sensitization of the effects of nicotine on energy balance. Herein, we explore this hypothesis, and we scrutinize the molecular crosstalk between nAChR and GLP-1R signaling in brain regions involved in regulation of homeostatic and reward-based feeding.



## RESULTS

### GLP-1 and nicotine co-treatment reverses metabolic abnormalities in obese mice

To determine the therapeutic effects of nicotine and GLP-1 combination therapy on energy balance, we treated diet-induced obese (DIO) mice once daily with nicotine (1 mg/kg), the pharmacokinetically optimized GLP-1R agonist liraglutide (10 nmol/kg), co-administration of both (nicotine [1 mg/kg] and liraglutide [10 nmol/kg]), or vehicle over the course of 16 days (Figure 1A). The study was conducted at submaximal doses of the compounds to ensure a therapeutic window with opportunity for evaluating weight loss additivity or synergy.<sup>14,20</sup> The co-administration treatment synergistically lowered body weight over 16 days relative to the individual monotherapies (Figures 1B and 1C). Assessment of body composition showed that the additional weight loss from co-administration treatment was primarily governed by a reduction in fat mass with a minor reduction in lean mass (Figure 1D). A significant reduction in food intake over the course of the 16-day study showed that the weight loss following treatment with the combination of liraglutide and nicotine is, at least partially, driven by potentiated anorexia (Figures 1E and 1F). To gain insight into whether also an increase in energy expenditure is contributing to the observed weight loss following treatment with the co-administration, we conducted a 16-day pair-feeding study in DIO mice (Figure 1G). Co-administration resulted in a pronounced weight loss in DIO mice, which was significantly greater compared with the pair-feeding control group, suggesting a contribution from increased energy expenditure to the weight loss (Figures 1H and 1I). These findings were corroborated by the observation of an increase in uncoupling protein-1 (UCP-1) immunoreactivity in inguinal white adipose tissue (iWAT) indicative of increased thermogenic capacity (Figures 1J and 1K). Collectively, these findings suggest that co-administration of liraglutide and nicotine synergistically lowers body weight through concerted actions on energy expenditure and food intake.

The pronounced weight loss following co-administration of liraglutide and nicotine also coincided with several metabolic benefits. Mice treated with the drug combination displayed improved insulin sensitivity (Figures 1L, S1A, and S1B), and reductions in white adipocyte size and lipid content in the liver and brown adipose tissue (Figures S1C–S1H). Importantly, no differences in general locomotor activity or behavior were observed in response to any of the treatments (Figures 1M and 1N). This was further corroborated by a chronic treatment study in chow-fed lean mice. The lean mice defended their weight against the pharmacological treatments and displayed no sign of aberrant behavior assessed by an open field test (Figures S1I–S1N). Notably, the weight lowering and hypophagic effects of the co-treatment were similar in DIO nAChR  $\beta_4$  knockout (KO) and DIO wild-type mice, suggesting that the crosstalk between nAChRs and GLP-1R implicates pathways independent of  $\beta_4$ -containing nAChRs (Figures S1O–S1Q).

### Homeostatic and hedonic brain circuits are engaged by nicotine and liraglutide co-treatment

Given that both the GLP-1R and nAChRs are expressed throughout the mammalian brain, we performed unbiased

whole-brain c-Fos three-dimensional imaging to map the global neuronal activity signature in response to a single administration of either vehicle, nicotine, liraglutide or co-administration in DIO mice (Figure 2A). Interestingly, liraglutide and nicotine co-administration seemed to reciprocally potentiate the neuronal response to each individual compound across multiple brain areas involved in body weight regulation (Figures 2B–2F and S2A–S2L), in agreement with the synergistic relationship observed from the pharmacological weight loss studies. Nicotine treatment led to increased neuronal activity in brainstem (area postrema [AP], nucleus of the solitary tract [NTS], and dorsal motor nucleus of the vagus nerve [DMX]), dorsomedial nucleus of the hypothalamus (DMH), ventral tegmental area (VTA), and paraventricular hypothalamic nucleus (PVH), whereas liraglutide most prominently engaged neurocircuits in the brainstem and in the hypothalamus. In contrast, co-administration of nicotine and liraglutide potently induced c-Fos expression in all the designated sub-regions of the hypothalamus (PVH, DMH, arcuate nucleus of the hypothalamus [ARC], and lateral hypothalamic area [LHA]), as well as in three designated sub-regions of the brainstem (NTS, DMX, and parabrachial nucleus [PB]), the VTA, the nucleus accumbens (NAc), and the central amygdala (CEA). Together, these data indicate that simultaneous activation of GLP-1R and nAChRs powerfully engages several brain regions, and that the synergistic pharmacological weight loss benefits may emerge as a consequence of increased neuronal crosstalk between homeostatic and hedonic pathways in brain regions involved in appetite regulation.

### Effect of GLP-1 and nicotine co-treatment on POMC neurons

The individual pharmacological effects of nicotine and liraglutide on body weight have been, at least partially, attributed to direct activation of POMC neurons situated in the ARC.<sup>13,21,22</sup> Consistent with these findings, our c-Fos data demonstrate that co-treatment synergistically increases neuronal activity in the arcuate nucleus (Figures 3A–3C), implying that the enhanced weight loss efficacy may be consequential to coordinated activation of POMC neurons. To elucidate whether the GLP-1R may serve as a sensitizer to potentiate the neuronal activity of nicotine pharmacology, we performed brain-slice electrophysiological recordings on immune-validated POMC neurons from ARC (Figures 3D and S3A). Bath application of liraglutide had no effect on the membrane potential, whereas puff application of nicotine led to depolarization of ARC POMC neurons. Co-application of liraglutide and nicotine increased POMC excitability and firing rate, signifying that liraglutide sensitizes POMC neurons to nicotine. The potentiation of neuronal excitability to nicotine by liraglutide is evident from the observation that liraglutide itself increases the frequency, number, and amplitude of spontaneous excitatory post-synaptic events (Figures 3E–3H). Next, dynamic changes in intracellular calcium were assessed, using single-cell fluorescence imaging. Application of liraglutide evoked a slow and progressive increase in intracellular calcium transients, whereas nicotine led to an acute and rapid response (Figures 3I, 3J, S3B, and S3C). When nicotine was applied at the plateau of the liraglutide response, the calcium influx was significantly augmented, corroborating that GLP-1R agonism sensitizes POMC neurons to nicotinic actions.

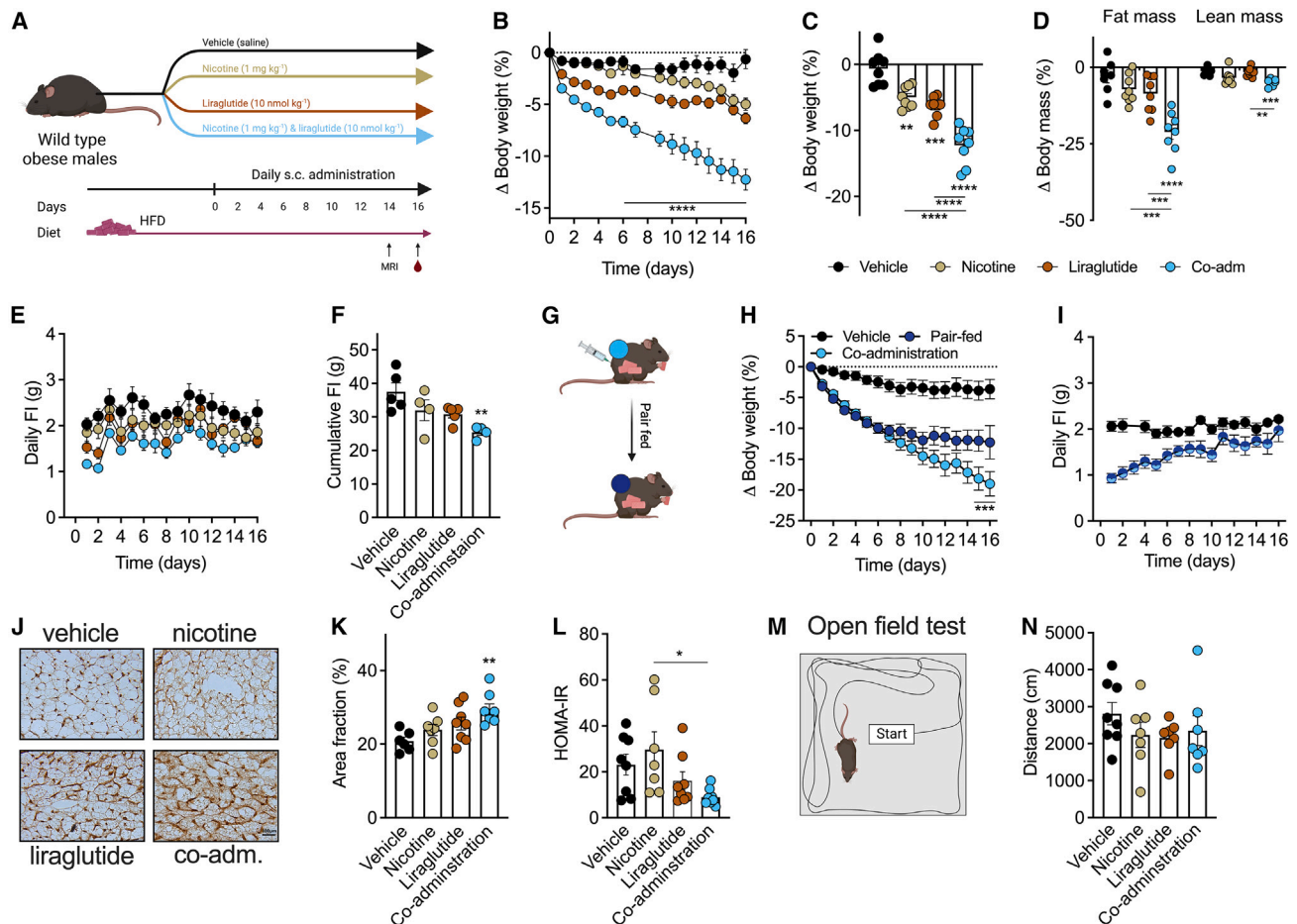


**Figure 1. Liraglutide and nicotine combination therapy lowers body weight in obese mice**

(A) Illustration of study in high-fat-diet (HFD)-induced obese C57BL/6J male mice treated with once-daily subcutaneous (s.c.) injections of vehicle, liraglutide 10 nmol/kg, nicotine 1 mg/kg, or co-administration of liraglutide 10 nmol/kg and nicotine 1 mg/kg for 16 days.

(B) Change in body weight ( $n = 8$ , biological replicates). Data were analyzed by two-way RM ANOVA with Bonferroni multiple comparison test, \*\*\*\* $p < 0.0001$  comparing co-administration and liraglutide treatment groups.

(C) Change in body weight at day 16 ( $n = 8$ , biological replicates). Data were analyzed by one-way ANOVA with Bonferroni multiple comparison test, \*\* $p < 0.01$ , \*\*\* $p < 0.001$ , \*\*\*\* $p < 0.0001$ .

(D) Change in body composition ( $n = 7-8$ , biological replicates). One mouse was excluded in the vehicle group because of technical error in data acquisition. Data were analyzed by two-way RM ANOVA with Bonferroni multiple comparison test, \*\* $p < 0.01$ , \*\*\* $p < 0.001$ , \*\*\*\* $p < 0.0001$ .

(E) Daily food intake ( $n = 4-5$ , biological replicates). Data were analyzed by two-way RM ANOVA with Bonferroni multiple comparison test.

(F) Cumulative food intake at day 16 ( $n = 4-5$ , biological replicates). Data were analyzed by one-way ANOVA with Bonferroni multiple comparison test, \*\* $p < 0.01$ .

(G) Illustration of pair-feeding study in HFD-induced obese C57BL/6J male mice treated with once-daily s.c. injections of vehicle or co-administration of liraglutide 10 nmol/kg and nicotine 1 mg/kg, and a group pair-fed to the co-administration group for 16 days.

(H) Change in body weight ( $n = 8$ , biological replicates). Data were analyzed by two-way RM ANOVA with Bonferroni multiple comparison test, \*\*\* $p < 0.001$  comparing co-administration and pair-fed groups.

(I) Daily food intake ( $n = 4-5$ , biological replicates). Data from vehicle and one mouse in co-treatment group were excluded because of technical error in food intake measurements. Data were analyzed by two-way RM ANOVA with Bonferroni multiple comparison test.

(J) Representative images showing UCP-1 immunoreactivity in iWAT from mice in study in (A). Scale bar, 100  $\mu\text{m}$ .

(K) Quantification of immunoreactivity in (J) ( $n = 6-8$ , biological replicates). Data were not collected from two samples in vehicle and one sample in nicotine group because of low sample quality. Data were analyzed by one-way ANOVA with Bonferroni multiple comparison test, \*\* $p < 0.01$ .

(L) HOMA-IR (homeostasis model assessment of insulin resistance) measurements at day 16 from mice in (A) ( $n = 7-8$ , biological replicates). One sample in nicotine group was not calculated because of non-determinable plasma insulin levels. Data were analyzed by one-way ANOVA with Bonferroni multiple comparison test, \*\* $p < 0.01$ .

(M) Illustration of open field test in HFD-induced obese C57BL/6J male mice treated with a single s.c. injection of vehicle, liraglutide 10 nmol/kg, nicotine 1 mg/kg, or co-administration of liraglutide 10 nmol/kg and nicotine 1 mg/kg.

(N) Distance traveled during 10 min of open field test ( $n = 7-8$ , biological replicates). Data were analyzed by one-way ANOVA with Bonferroni multiple comparison test. All data are reported as mean  $\pm$  SEM.

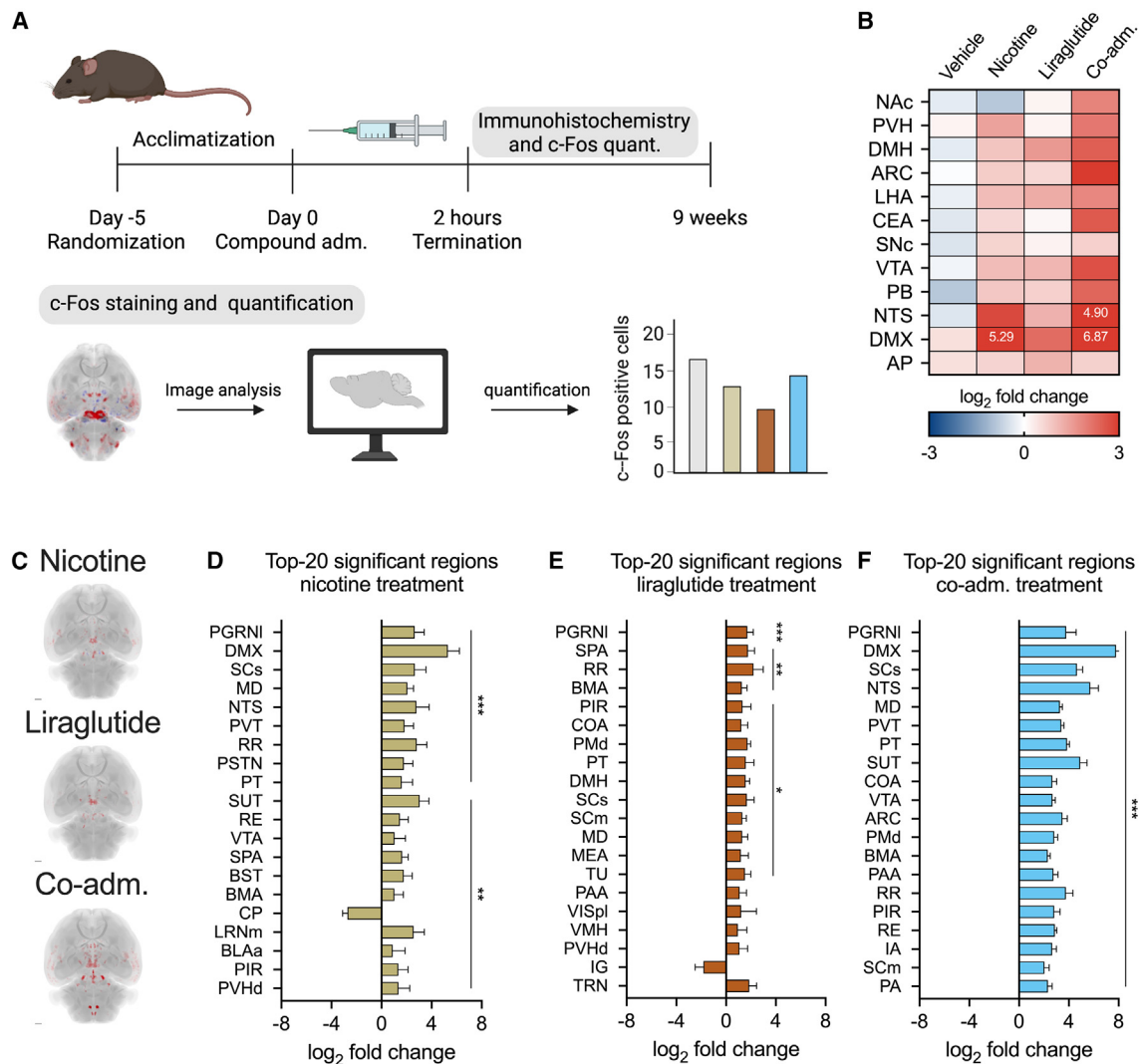


**Figure 2. Three-dimensional whole-brain activity signature in response to liraglutide and nicotine co-treatment**

(A) Illustration of study in HFD-induced obese C57BL/6J male mice treated with a single s.c. injection of vehicle, liraglutide 10 nmol/kg, nicotine 1 mg/kg, or co-administration of liraglutide 10 nmol/kg and nicotine 1 mg/kg. Brains were harvested 2 h after injection and subjected to tissue clearing, c-Fos immunohistochemistry, and quantification.

(B) Heatmap showing  $\log_2$  fold changes in c-Fos expression in common brain areas involved in appetite regulation relative to vehicle ( $n = 5-7$ , biological replicates). Numerical values outside the scale are denoted on the figure.

(C) Dorsal view of heatmap showing regulated brain regions in response to treatments.

(D) Top 20 regulated brain areas in response to a single injection of 1 mg/kg nicotine treatment represented as  $\log_2$  fold change relative to vehicle ( $n = 7$ , biological replicates). Data were analyzed by one-way ANOVA, multiple comparison, Dunnett's post hoc test, negative binomial generalized linear model in comparison with vehicle group, \*\* $p < 0.01$ , \*\*\* $p < 0.001$  comparing compound injections with vehicle.

(E) Top 20 regulated brain areas in response to a single injection of 10 nmol/kg liraglutide treatment represented as  $\log_2$  fold change relative to vehicle ( $n = 6$ , biological replicates). Data were analyzed by one-way ANOVA, multiple comparison, Dunnett's post hoc test, negative binomial generalized linear model in comparison with vehicle group, \* $p < 0.05$ , \*\* $p < 0.01$ , \*\*\* $p < 0.001$ .

(F) Top 20 regulated brain areas in response to a single injection of 10 nmol/kg liraglutide treatment represented as  $\log_2$  fold change relative to vehicle ( $n = 7$ , biological replicates). Data were analyzed by one-way ANOVA, multiple comparison, Dunnett's post hoc test, negative binomial generalized linear model in comparison with vehicle group, \*\*\* $p < 0.001$ .

Brain region abbreviations can be found in [STAR Methods](#) section "unbiased whole-brain c-Fos imaging". All data are reported as mean  $\pm$  SEM.

To further understand the molecular crosstalk between coordinated activation of GLP-1R and nAChRs, we performed unbiased transcriptional profiling (bulk mRNA sequencing) of ARC microdissected from DIO mice treated with nicotine, liraglutide, co-adminis-

tration, or vehicle for 3 days (Figures 3K and S3D). After adjusting for multiple testing, no significantly regulated transcripts were detected following nicotine treatment. In contrast, 8 transcripts were significantly regulated by liraglutide treatment, and 538 transcripts

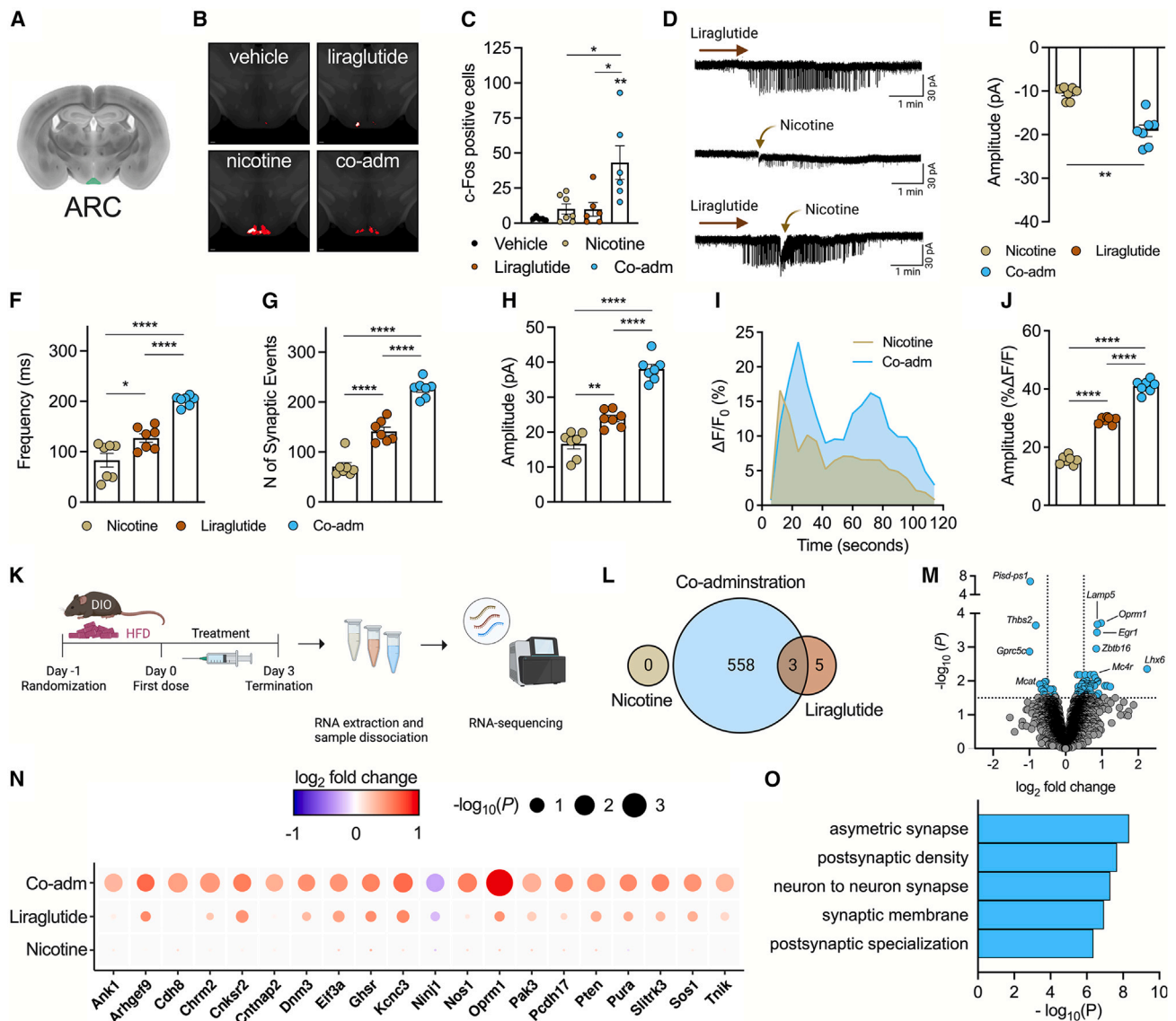


**Figure 3. Coordinated GLP-1R and nicotinic receptor agonism increases neuronal activity in the ARC**

(A) Coronal view of mouse brain with the arcuate nucleus (ARC) highlighted.

(B) Coronal view of representative images of c-Fos expression profiles in ARC from unbiased whole-brain c-Fos expression imaging of HFD-induced obese C57BL/6J male mice treated with a single s.c. injection of vehicle, liraglutide 10 nmol/kg, nicotine 1 mg/kg, or co-administration of liraglutide 10 nmol/kg and nicotine 1 mg/kg. Brains were harvested 2 h after injection and subjected to tissue clearing, c-Fos immunohistochemistry, and quantification.

(C) Quantification of c-Fos-positive cells in ARC (n = 5–7, biological replicates). Data were analyzed by one-way ANOVA with Bonferroni multiple comparison test, \*p < 0.05, \*\*p < 0.01.

(D) Representative voltage-clamp recordings of POMC<sup>+</sup> neurons identified by immunohistochemistry from microdissected ARC brain slices in response to bath application of 100 nM liraglutide, puff application of 10 μM nicotine, or combined bath application of 100 nM liraglutide and puff application of 10 μM nicotine. (E) Amplitude changes in inward current induced by nicotine (n = 7, technical replicates). Data were analyzed by paired t test with two-tailed comparison test, \*\*p < 0.01.

(F) Changes in synaptic events frequency (n = 7, technical replicates). Data were analyzed by one-way ANOVA with Bonferroni multiple comparison test, \*p < 0.05, \*\*\*\*p < 0.0001.

(G) Number of synaptic events (n = 7, technical replicates). Data were analyzed by one-way ANOVA with Bonferroni multiple comparison test, \*\*\*\*p < 0.0001.

(H) Changes in amplitude of synaptic events (n = 7, technical replicates). Data were analyzed by one-way ANOVA with Bonferroni multiple comparison test, \*\*p < 0.01, \*\*\*\*p < 0.0001.

(I) Representative Ca<sup>2+</sup> imaging recordings of POMC<sup>+</sup> neurons identified by immunohistochemistry from microdissected ARC brain slices in response to bath application of 100 nM liraglutide, puff application of 10 μM nicotine, or combined bath application of 100 nM liraglutide and puff application of 10 μM nicotine. (J) Area under the curve from Ca<sup>2+</sup> imaging (n = 7, technical replicates). Data were analyzed by one-way ANOVA with Bonferroni multiple comparison test, \*\*\*\*p < 0.0001.

(legend continued on next page)

were regulated following the co-treatment (Figure 3L). Using a volcano plot to visualize the top transcripts regulated in response to the co-treatment with nicotine and liraglutide, we identified a number of top regulated hits with well-established roles in energy balance regulation, including *Egr1*, *Oprm1*, and *Mc4r*<sup>23–25</sup> (Figure 3M). Pathway analyses of the enriched genes indicated that the synergistic metabolic effects of co-treatment of liraglutide and nicotine may involve changes in neuroplasticity in the ARC as envisaged from the top Gene Ontology (GO) terms (Figure 3N). Finally, visualization of the top 20 most enriched transcripts underlying the top five GO terms further emphasized the powerful molecular crosstalk between GLP-1 and nicotine pharmacology (Figure 3O). The functional importance of GLP-1R signaling in the ARC was confirmed by pre-infusing the natural GLP-1R antagonist, exendin 9-39, directly into the ARC of DIO mice immediately prior to co-treatment with liraglutide and nicotine. Pharmacologically blocking the GLP-1R in the ARC attenuated the weight loss efficacy of the combination therapy (Figures S3E–S3H), suggesting that the weight-lowering effects are partially driven by hypothalamic GLP-1R signaling.

#### Liraglutide and nicotine co-treatment augments dopaminergic reward signaling

The unbiased assessment of whole-brain neuronal activity revealed that co-treatment with nicotine and liraglutide also engages brain regions associated with food reward, including the VTA (Figures 4A–4C). Activation of the mesolimbic dopaminergic reward pathway is central to the rewarding value of nicotine, including its addictive properties.<sup>26</sup> Similarly, there is evidence supporting both direct and indirect actions of GLP-1R to modulate dopaminergic projections from the VTA to NAc.<sup>27</sup> Complementary to the experiments on ARC POMC neurons, we used slice electrophysiology to evaluate the effects of nicotine and liraglutide and the combination of the two molecules on dopaminergic neuronal activity in the VTA (Figure 4D). Bath application of liraglutide did not affect membrane potential, whereas application of nicotine led to depolarization of VTA dopaminergic neurons. GLP-1R agonists have previously been reported to induce membrane depolarization,<sup>22</sup> but this might be dose related and here we show that 100 nM liraglutide does not elicit changes in synaptic current. However, upon co-application of liraglutide and nicotine, an increase in dopaminergic excitability, amplitude, and firing rate was observed relative to the monoagonist control applications, signifying that liraglutide sensitizes dopaminergic neurons to nicotine actions in the VTA (Figures 4E–4H). Next, we used calcium imaging to probe dynamic changes in intracellular calcium levels in VTA neurons and found that co-application gave rise to a significant increase in calcium levels in dopaminergic neurons in the VTA relative to the respective monotherapies (Figures 4I, 4J, S4A, and S4B). The

fact that depolarization was uncoupled from the elevated intracellular calcium levels suggests that the calcium influx could be mediated via AMPA receptors rather than voltage-gated calcium channels. To delineate a possible functional contribution from AMPA receptors, we infused the AMPA receptor antagonist, NBQX, directly into the VTA prior to subcutaneous administration of nicotine and liraglutide, and we found that pharmacological antagonism of VTA AMPA receptor signaling attenuated the weight-lowering effects of nicotine and liraglutide co-treatment (Figures S4C–S4F). Next, we explored the necessity of VTA GLP-1R signaling for the weight loss benefits of nicotine and liraglutide co-treatment by infusion of the GLP-1R antagonist exendin 9-39 to the VTA (Figures S4G–S4J). Pre-infusion with exendin 9-39 substantially attenuated the effect of the co-administration to lower body weight, emphasizing that the anti-obesity benefits of liraglutide and nicotine co-treatment implicate GLP-1R in the mesolimbic reward system.

#### GLP-1 counteracts nicotine-induced dopamine signaling in the NAc

To further characterize the pharmacological effects of nicotine and liraglutide co-administration treatment on the mesolimbic reward system, we evaluated the neuronal response in the NAc. Our unbiased whole-brain imaging data revealed a significant increase in c-Fos in the NAc exclusively following the combination therapy (Figures 5A–5C). This prompted us to dissect the functional consequences of the pharmacological intervention on NAc dopamine signaling *in vivo*, by viral-mediated expression of the genetically encoded dopamine sensor dLight1.3b for optical detection of acute dopamine release (Figures 5D and S5).<sup>28,29</sup> Nicotine administration elicited a rapid and sustained increase in dLight1.3b fluorescence consistent with an increase in NAc dopamine release. Interestingly, the nicotine-induced increase was dampened by co-treatment with liraglutide that by itself had no influence on the fluorescent signal (Figures 5E and 5F). Whether these opposing actions of GLP-1R agonism and nicotine on mesolimbic dopaminergic reward signaling *in vivo* are important for weight loss benefits of their combined treatment remains to be addressed. Further, it could be speculated that the GLP-1R-induced blunting of nicotine-induced dopamine signaling in the NAc may circumvent some of the addictive properties of nicotine and thus enhance the safety profile of the combination approach.<sup>26,30</sup>

#### DISCUSSION

In this study, we demonstrate that combinatorial treatment with nicotine and the long-acting GLP-1R agonist, liraglutide,

(K) Illustration of bulk RNA sequencing study of microdissected ARC nuclei from HFD-induced obese C57BL/6J male mice treated with s.c. injections of vehicle, liraglutide 10 nmol/kg, nicotine 1 mg/kg, or co-administration of liraglutide 10 nmol/kg and nicotine 1 mg/kg for 3 days. Brains were harvested 2 h after the final injection on day 3 (n = 5–6, biological replicates).

(L) Venn diagram presentation of differentially expressed genes in response to treatment relative to vehicle. Benjamini-Hochberg adjusted p < 0.05.

(M) Volcano plot for differentially expressed genes in response to liraglutide 10 nmol/kg and nicotine 1 mg/kg co-administration relative to vehicle. Light blue represents a Benjamini-Hochberg adjusted p < 0.05. Light gray represents an Benjamini-Hochberg adjusted p < 0.05. Selected genes are labeled.

(N) Top 20 differentially expressed genes within top 5 GO terms in (O). Dot size indicates the significance level. Dot color indicates the log<sub>2</sub> fold change.

(O) Top five most enriched GO terms for the 558 uniquely differentially expressed genes between co-administration of liraglutide 10 nmol/kg and nicotine 1 mg/kg treatment group and vehicle. All data are reported as mean ± SEM.

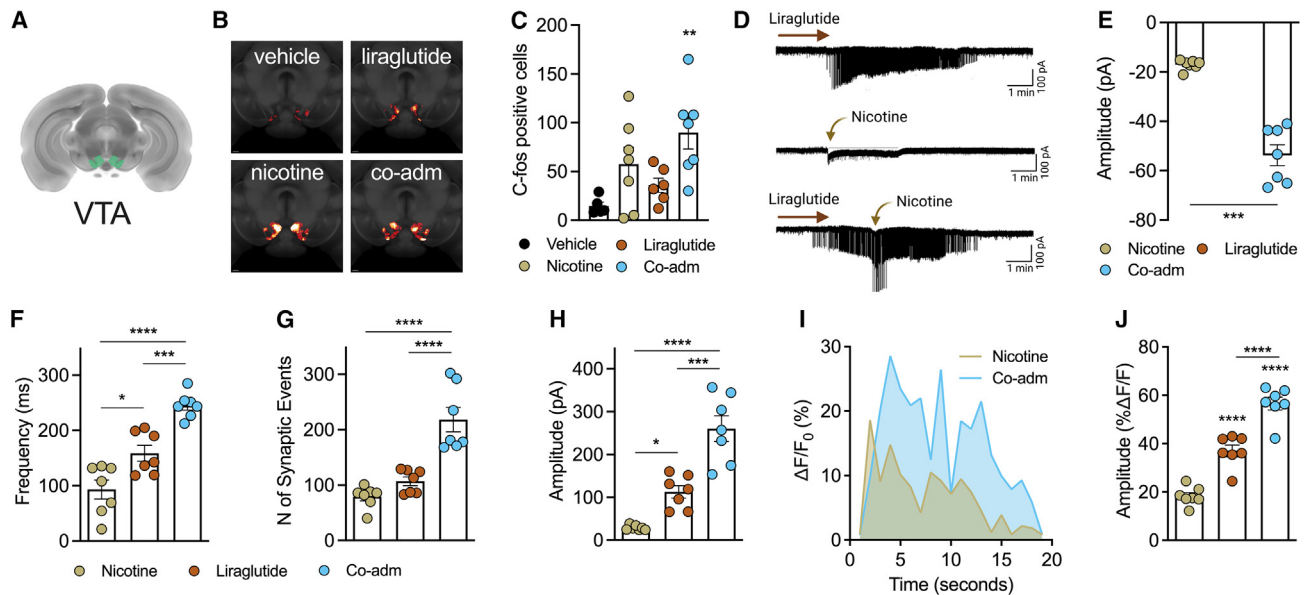


**Figure 4. Coordinated GLP-1R and nicotinic receptor agonism potentiates the activity of dopamine neurons in the ventral tegmental area (VTA)**

(A) Coronal view of mouse brain with the VTA highlighted.

(B) Coronal view of representative images of c-Fos expression profiles in VTA from unbiased whole-brain c-Fos expression imaging of HFD-induced obese C57BL/6J male mice treated with a single s.c. injection of vehicle, liraglutide 10 nmol/kg, nicotine 1 mg/kg, or co-administration of liraglutide 10 nmol/kg and nicotine 1 mg/kg. Brains were harvested 2 h after injection and subjected to tissue clearing, c-Fos immunohistochemistry, and quantification.

(C) Quantification of c-Fos-positive cells in VTA (n = 5–7, biological replicates). Data were analyzed by one-way ANOVA with Bonferroni multiple comparison test, \*\*p < 0.01.

(D) Representative voltage-clamp recordings of microdissected VTA brain slices in response to bath application of 100 nM liraglutide, puff application of 10  $\mu$ M nicotine, or combined bath application of 100 nM liraglutide and puff application of 10  $\mu$ M nicotine.

(E) Amplitude changes in inward current induced by nicotine (n = 7, technical replicates). Data were analyzed by paired t test with two-tailed comparison test, \*\*\*p < 0.01.

(F) Changes in synaptic events frequency (n = 7, technical replicates). Data were analyzed by one-way ANOVA with Bonferroni multiple comparison test, \*p < 0.05, \*\*\*p < 0.001, \*\*\*\*p < 0.0001.

(G) Number of synaptic events (n = 7, technical replicates). Data were analyzed by one-way ANOVA with Bonferroni multiple comparison test, \*\*\*\*p < 0.0001.

(H) Changes in amplitude of synaptic events (n = 7, technical replicates). Data were analyzed by one-way ANOVA with Bonferroni multiple comparison test, \*p < 0.05, \*\*\*p < 0.001, \*\*\*\*p < 0.0001.

(I) Representative Ca<sup>2+</sup> imaging recordings of POMC<sup>+</sup> neurons identified by immunohistochemistry from microdissected ARC brain slices in response to bath application of 100 nM liraglutide, puff application of 10  $\mu$ M nicotine, or combined bath application of 100 nM liraglutide and puff application of 10  $\mu$ M nicotine.

(J) Area under the curve from Ca<sup>2+</sup> imaging (n = 7, technical replicates). Data were analyzed by one-way ANOVA with Bonferroni multiple comparison test, \*\*\*\*p < 0.0001. All data are reported as mean  $\pm$  SEM.

synergistically reverses obesity and metabolic defects in mice. The pronounced negative energy balance elicited by combining nicotine and liraglutide is mediated by dual effects on food intake and energy expenditure. Using whole-brain three-dimensional imaging, electrophysiology, transcriptomics, and fiber photometry, we reveal neuronal and molecular crosstalk between nicotine and GLP-1R agonism in brain regions linked to homeostatic regulation of food intake and in the mesolimbic reward pathway. These findings suggest a therapeutic potential associated with introducing nicotinic receptor agonism as an adjunct to GLP-1R agonism for the treatment of metabolic diseases. The rationale for pursuing metabolic benefits of combined nicotinic receptor agonism and GLP-1R agonism is supported by previous work identifying GLP-1 as a nicotine-sensitizing agent.<sup>19</sup> In agreement, we here identify several layers of signaling crosstalk between liraglutide and nicotine. By using whole-brain three-dimensional imaging, we demon-

strate that when nicotine and liraglutide are co-administered, the signaling properties of each compound appear to be mutually potentiated in key feeding regions important for regulation of both homeostatic feeding (ARC) and reward (VTA and NAc)-based feeding behavior. We go on to demonstrate that GLP-1R agonism increases neuronal excitability to nicotine in both hypothalamic POMC neurons and in dopaminergic neurons in the VTA, and we further establish functional interaction between GLP-1R signaling and nicotinic signaling in the NAc. It remains to be determined, however, if the liraglutide-mediated inhibition of nicotine-induced dopaminergic signaling in the NAc is contributing to the weight-lowering benefits of the combination. Also, because nicotine's effect on dopamine neurons in the VTA is considered key to the rewarding and addictive aspects of smoking,<sup>26,31,32</sup> another fascinating probability is that liraglutide appropriately circumvents this vice of nicotine administration.

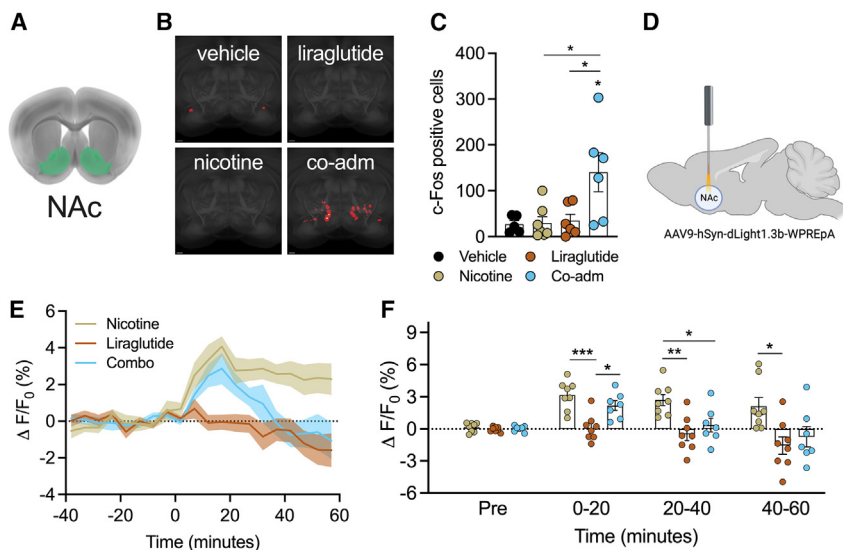


**Figure 5. Liraglutide attenuates nicotine-induced dopamine release in nucleus accumbens (NAc)**

(A) Coronal view of mouse brain with the NAc highlighted.

(B) Coronal view of representative images of c-Fos expression profiles in NAc from unbiased whole-brain c-Fos expression imaging of HFD-induced obese C57BL/6J male mice treated with a single s.c. injection of vehicle, liraglutide 10 nmol/kg, nicotine 1 mg/kg, or co-administration of liraglutide 10 nmol/kg and nicotine 1 mg/kg. Brains were harvested 2 h after injection and subjected to tissue clearing, c-Fos immunohistochemistry, and quantification.

(C) Quantification of c-Fos-positive cells in NAc ( $n = 5-7$ , biological replicates). Data were analyzed by one-way ANOVA with Bonferroni multiple comparison test,  $*p < 0.05$ .

(D) Illustration of study showing viral expression of adeno-associated virus serotype 9 (AAV9)-hSyn-dLight1.3b and fiber photometry recording of dopamine in NAc from mice receiving a single s.c.

injection of liraglutide 10 nmol/kg, nicotine 1 mg/kg, or co-administration of liraglutide 10 nmol/kg and nicotine 1 mg/kg.

(E) Real-time *in vivo* recording of dopamine release before and after compound administration at  $t = 0$  ( $n = 7-8$ , biological replicates). Signal normalized to a 20-min period immediately before injection of experimental compounds. Shaded area indicates  $\pm$ SEM.

(F) Mean  $\Delta F/F_0$  traces before and after administration of experimental compounds represented as 20-min intervals ( $n = 7-8$ , biological replicates). Signal normalized to a 20-min period immediately before injection of experimental compounds. Data were analyzed by one-way ANOVA within each time point with Bonferroni multiple comparison test,  $*p < 0.05$ ,  $**p < 0.01$ ,  $***p < 0.001$ . All data are reported as mean  $\pm$  SEM.

One challenge associated with targeting nicotinic receptors for metabolic disease is the fact that nicotine consumption has been associated with hyperglycemia and increased risk of type 2 diabetes.<sup>33</sup> Importantly, GLP-1R agonism counterbalances any potential metabolic adverse effects of nicotine, demonstrated by improved insulin sensitivity and reduction in hepatic fat content following the combined treatment. Whether the effect of GLP-1 to counter metabolic derangements of nicotine implicates targeting of a previously identified habenula-pancreas axis linking nicotine consumption to hyperglycemia remains to be determined,<sup>34</sup> but it is plausible based on the known actions of GLP-1R signaling in the habenula.<sup>19</sup>

Although our data support a combinatorial use of nicotine with a GLP-1R agonist for treatment of obesity and its associated metabolic complications, nicotine is not an appropriate weight loss drug candidate. However, given that  $\sim 1.3$  billion people already self-administer nicotine in the form of tobacco,<sup>35</sup> it should be intriguing to explore whether smokers with obesity respond particularly well to the weight-lowering effects of GLP-1R agonists. Indeed, pharmaceutical companies with clinical GLP-1 programs may already have access to data that allow stratification of weight loss data based on smoking status, distinguishing between smokers and non-smokers. If such a post hoc analysis supports translational benefits of combining nicotine with GLP-1R agonism, the motivation for further drug development to engineer safe and efficacious nAChR agonists might be heightened. In context, we have previously rationalized that agonists specifically targeting  $\beta_4$ -containing nAChR subtypes<sup>14,36</sup> may be advantageous for treatment of obesity and diabetes. Unexpectedly, we found in this study that the metabolic effects of combined liraglutide and nicotine treatment emerge independently of  $\beta_4$ -containing nAChRs, underlining

that other nAChR subtypes are governing the interaction with GLP-1R signaling to drive weight loss. The safety of future nAChR-targeting approaches could be bolstered by employing tissue-targeting approaches, for example, by using GLP-1<sup>37,38</sup> to deliver nAChR small molecule ligands specifically to GLP-1R-positive neurons.<sup>39</sup> Whereas a restricted delivery of nicotinic receptor agonists might compromise some of the wide-ranging metabolic benefits of the two compounds when co-administered, it potentially solves the concerns pertaining to unwanted effects of nicotinic receptor ligands.

Pharmacological approaches that safely target motivational aspects of feeding and palatable food reward have been a key focus area for weight loss research for decades. For example, naltrexone/bupropion combination has been promoted to exhibit dual effects on satiety and food reward.<sup>40</sup> However, the discontinuation of rimonabant, a type 1 cannabinoid receptor (CB1R) antagonist, as a result of severe adverse psychiatric effects,<sup>41</sup> serves as an important reminder to carefully ensure that the pharmacological benefits on reward and motivation are uncoupled from adverse effects on anxiety and mood. It is increasingly evident that hypothalamic circuits are interconnected with midbrain-controlled motivation,<sup>42</sup> and that exposure to a palatable diet devalues a healthy diet through mechanisms involving both hypothalamic and mesolimbic circuits.<sup>43</sup> Accordingly, it might be possible to dampen food reward indirectly through targeting receptors in the hypothalamus and/or in the brainstem. The data presented here support that the combination of nicotine and GLP-1 could exert both direct and indirect actions on neurons in the hypothalamus, brainstem, and VTA.

In summary, we demonstrate neuronal cross-sensitization between nicotinic receptor agonism and GLP-1R agonism and show that this neurobiological interplay can be exploited

pharmacologically for the treatment of obesity in preclinical models. Of note, we reveal that coordinated targeting of nAChRs and GLP-1Rs lowers body weight via pathways involving appetite suppression, reward modulation, and increased energy expenditure. Critical translational work lies ahead in determining whether nicotinic receptor targeting holds promise to safely potentiate weight loss efficacy of GLP-1-based therapies in patients with obesity.

### Limitations of the study

The data presented here suggest that the metabolic benefits from liraglutide and nicotine co-treatment are consequential to molecular synergy across multiple brain regions. Although we functionally validate the contribution from GLP-1R signaling in ARC and VTA, several unknowns regarding the neurocircuitry and molecular mechanisms of action are left unaddressed. For example, it may be that the drug-induced effects on dopaminergic signaling in the NAC are consequential to feedforward signaling propagated from the brainstem or the hypothalamus. This should be evaluated in future studies. Additional experiments are also required to determine the implications of GLP-1R-induced attenuation of nicotine-induced dopamine release. Whereas we believe that this finding encourages further work on GLP-1R agonism for tobacco addiction, it does not necessarily reflect an essential interaction in the context of weight loss and metabolic disease. In contrast, it should be interesting to experimentally address whether chronic co-treatment with GLP-1 and nicotine alters the dopaminergic response to (palatable) food presentation, for example, following a period of food deprivation. Finally, high doses of nicotine can be aversive, and previous work has demonstrated that GLP-1R agonism promotes nicotine avoidance.<sup>19</sup> Thus, it cannot be excluded that the benefits on body weight loss following combined treatment with nicotine and GLP-1 are partially mediated through a potentiated aversive effect of both signals.

### STAR★METHODS

Detailed methods are provided in the online version of this paper and include the following:

- KEY RESOURCES TABLE
- RESOURCE AVAILABILITY
  - Lead contact
  - Materials availability
  - Data and code availability
- EXPERIMENTAL MODELS AND SUBJECT DETAILS
  - Animals
- METHOD DETAILS
  - Pharmacology
  - Pair-feeding
  - Body composition measurement
  - Tissue harvest and processing
  - Pathohistological analyses
  - Blood glucose and insulin measures
  - Open field test
  - Unbiased whole-brain c-Fos imaging
  - RNA sequencing

- ARC and VTA cannulations
- Adeno-associated viral (AAV) vector infusion and fiber optic cannula implantation
- *In vivo* dopamine release recordings
- Analysis of fiber photometry data
- Electrophysiology
- QUANTIFICATION AND STATISTICAL ANALYSES

### SUPPLEMENTAL INFORMATION

Supplemental information can be found online at <https://doi.org/10.1016/j.celrep.2023.112466>.

### ACKNOWLEDGMENTS

We thank the single-cell omics platform (SCOP) and the Rodent Metabolic Phenotyping Platform (RMPP) at the Novo Nordisk Foundation Center for Basic Metabolic Research (CBMR) for the technical expertise and support with RNA sequencing and *in vivo* studies. We thank members from the Clemmensen lab for fruitful discussions. We thank Dr. Uwe Maskos for providing the CHRN4 KO mice. This work was supported by the Lundbeck Foundation (fellowship R238-2016-2859 to C.C., grants R266-2017-4331 and R276-2018-792 to U.G.) and by the Novo Nordisk Foundation (grant NNF17OC0026114). The Novo Nordisk Foundation Center for Basic Metabolic Research is an independent Research Center, based at the University of Copenhagen, Denmark, and partially funded by an unconditional donation from the Novo Nordisk Foundation (<https://cbmr.ku.dk/>) (grant NNF18CC0034900). Cartoon figures were prepared using [BioRender.com](https://BioRender.com).

### AUTHOR CONTRIBUTIONS

S.F., J.P., and C.S. carried out *in vivo* pharmacology experiments. S.F. and N.K. performed brain infusion studies. S.F., J.P., and C.S. conducted *ex vivo* analyses. K.L. and O.D. performed histology. G.S., U.R., and J.H.-S. performed the unbiased whole-brain c-Fos labeling and quantification. S.H.J., A.L.E., and U.G. performed and analyzed fiber photometry experiments. C.R.R.-L. and K.A.K. performed slice electrophysiology. M.Q.L., D.A.G.N., and T.H.P. performed bioinformatics. S.F., J.P., and C.C. analyzed the data. S.F., J.P., and C.C. wrote the manuscript.

### DECLARATION OF INTERESTS

J.P. and C.C. are co-founders of Ousia Pharma ApS, a biotech company developing therapeutics for treatment of metabolic disease.

Received: October 5, 2022

Revised: March 22, 2023

Accepted: April 18, 2023

Published: May 5, 2023

### REFERENCES

1. WHO (2023). World Health Organisation. [https://s3-eu-west-1.amazonaws.com/wof-files/World\\_Obesity\\_Atlas\\_2022.pdf](https://s3-eu-west-1.amazonaws.com/wof-files/World_Obesity_Atlas_2022.pdf).
2. Fontaine, K.R., Redden, D.T., Wang, C., Westfall, A.O., and Allison, D.B. (2003). Years of life lost due to obesity. *JAMA* 289, 187–193. <https://doi.org/10.1001/jama.289.2.187>.
3. Prospective Studies Collaboration; Whitlock, G., Lewington, S., Sherliker, P., Clarke, R., Emberson, J., Halsey, J., Qizilbash, N., Collins, R., and Peto, R. (2009). Body-mass index and cause-specific mortality in 900 000 adults: collaborative analyses of 57 prospective studies. *Lancet* 373, 1083–1096. [https://doi.org/10.1016/S0140-6736\(09\)60318-4](https://doi.org/10.1016/S0140-6736(09)60318-4).
4. Berrington de Gonzalez, A., Hartge, P., Cerhan, J.R., Flint, A.J., Hannan, L., MacInnis, R.J., Moore, S.C., Tobias, G.S., Anton-Culver, H., Freeman, L.B.,

- et al. (2010). Body-mass index and mortality among 1.46 million white adults. *N. Engl. J. Med.* 363, 2211–2219. <https://doi.org/10.1056/NEJMoa1000367>.
5. Garvey, W.T., Batterham, R.L., Bhatta, M., Buscemi, S., Christensen, L.N., Frias, J.P., Jódar, E., Kandler, K., Rigas, G., Wadden, T.A., et al. (2022). Two-year effects of semaglutide in adults with overweight or obesity: the STEP 5 trial. *Nat. Med.* 28, 2083–2091. <https://doi.org/10.1038/s41591-022-02026-4> (2022).
  6. Jastreboff, A.M., Aronne, L.J., Ahmad, N.N., Wharton, S., Connery, L., Alves, B., Kiyosue, A., Zhang, S., Liu, B., Bunck, M.C., et al. (2022). Tirzepatide once weekly for the treatment of obesity. *N. Engl. J. Med.* 387, 205–216. <https://doi.org/10.1056/NEJMoa2206038>.
  7. Petersen, J., Strömgaard, K., Frølund, B., and Clemmensen, C. (2019). Designing poly-agonists for treatment of metabolic diseases: challenges and opportunities. *Drugs* 79, 1187–1197. <https://doi.org/10.1007/s40265-019-01153-6>.
  8. Müller, T.D., Blüher, M., Tschöp, M.H., and DiMarchi, R.D. (2022). Anti-obesity drug discovery: advances and challenges. *Nat. Rev. Drug Discov.* 21, 201–223. <https://doi.org/10.1038/s41573-021-00337-8>.
  9. Enebo, L.B., Berthelsen, K.K., Kankam, M., Lund, M.T., Rubino, D.M., Salyganova, A., and Lau, D.C.W. (2021). Safety, tolerability, pharmacokinetics, and pharmacodynamics of concomitant administration of multiple doses of cagrilintide with semaglutide 2.4 mg for weight management: a randomised, controlled, phase 1b trial. *Lancet* 397, 1736–1748. [https://doi.org/10.1016/S0140-6736\(21\)00845-X](https://doi.org/10.1016/S0140-6736(21)00845-X).
  10. Clemmensen, C., Finan, B., Müller, T.D., DiMarchi, R.D., Tschöp, M.H., and Hofmann, S.M. (2019). Emerging hormonal-based combination pharmacotherapies for the treatment of metabolic diseases. *Nat. Rev. Endocrinol.* 15, 90–104. <https://doi.org/10.1038/s41574-018-0118-x>.
  11. Hsieh, M.T., Tseng, P.T., Wu, Y.C., Tu, Y.K., Wu, H.C., Hsu, C.W., Lei, W.T., Stubbs, B., Carvalho, A.F., Liang, C.S., et al. (2019). Effects of different pharmacologic smoking cessation treatments on body weight changes and success rates in patients with nicotine dependence: a network meta-analysis. *Obes. Rev.* 20, 895–905. <https://doi.org/10.1111/obr.12835>.
  12. Seoane-Collazo, P., Diéguez, C., Nogueiras, R., Rahmouni, K., Fernández-Real, J.M., and López, M. (2021). Nicotine' actions on energy balance: friend or foe? *Pharmacol. Ther.* 219, 107693. <https://doi.org/10.1016/j.pharmthera.2020.107693>.
  13. Mineur, Y.S., Abizaid, A., Rao, Y., Salas, R., DiLeone, R.J., Gündisch, D., Diano, S., De Biasi, M., Horvath, T.L., Gao, X.B., and Picciotto, M.R. (2011). Nicotine decreases food intake through activation of POMC neurons. *Science* 332, 1330–1332. <https://doi.org/10.1126/science.1201889>.
  14. Clemmensen, C., Jall, S., Kleinert, M., Quarta, C., Gruber, T., Reber, J., Sachs, S., Fischer, K., Feuchtinger, A., Karlas, A., et al. (2018). Coordinated targeting of cold and nicotinic receptors synergistically improves obesity and type 2 diabetes. *Nat. Commun.* 9, 4304. <https://doi.org/10.1038/s41467-018-06769-y>.
  15. Kroemer, N.B., Guevara, A., Vollstädt-Klein, S., and Smolka, M.N. (2013). Nicotine alters food-cue reactivity via networks extending from the hypothalamus. *Neuropsychopharmacology* 38, 2307–2314. <https://doi.org/10.1038/npp.2013.133>.
  16. Breum, A.W., Falk, S., Svendsen, C.S.A., Nicolaisen, T.S., Mathiesen, C.V., Maskos, U., and Clemmensen, C. (2022). Divergent roles of alpha5 and beta4 nicotinic receptor subunits in food reward and nicotine-induced weight loss in male mice. *Endocrinology* 163, bqac079. <https://doi.org/10.1210/endo/bqac079>.
  17. Lupien, J.R., and Bray, G.A. (1988). Nicotine increases thermogenesis in brown adipose tissue in rats. *Pharmacol. Biochem. Behav.* 29, 33–37. [https://doi.org/10.1016/0091-3057\(88\)90269-9](https://doi.org/10.1016/0091-3057(88)90269-9).
  18. Seoane-Collazo, P., Liñares-Pose, L., Rial-Pensado, E., Romero-Picó, A., Moreno-Navarrete, J.M., Martínez-Sánchez, N., Garrido-Gil, P., Iglesias-Rey, R., Morgan, D.A., Tomasini, N., et al. (2019). Central nicotine induces browning through hypothalamic kappa opioid receptor. *Nat. Commun.* 10, 4037. <https://doi.org/10.1038/s41467-019-12004-z>.
  19. Tuesta, L.M., Chen, Z., Duncan, A., Fowler, C.D., Ishikawa, M., Lee, B.R., Liu, X.A., Lu, Q., Cameron, M., Hayes, M.R., et al. (2017). GLP-1 acts on habenular avoidance circuits to control nicotine intake. *Nat. Neurosci.* 20, 708–716. <https://doi.org/10.1038/nn.4540>.
  20. Ratner, C., He, Z., Grunddal, K.V., Skov, L.J., Hartmann, B., Zhang, F., Feuchtinger, A., Bjerregaard, A., Christoffersen, C., Tschöp, M.H., et al. (2019). Long-acting neurotensin synergizes with liraglutide to reverse obesity through a melanocortin-dependent pathway. *Diabetes* 68, 1329–1340. <https://doi.org/10.2337/db18-1009>.
  21. He, Z., Gao, Y., Lieu, L., Afrin, S., Cao, J., Michael, N.J., Dong, Y., Sun, J., Guo, H., and Williams, K.W. (2019). Direct and indirect effects of liraglutide on hypothalamic POMC and NPY/AgRP neurons - implications for energy balance and glucose control. *Mol. Metab.* 28, 120–134. <https://doi.org/10.1016/j.molmet.2019.07.008>.
  22. Secher, A., Jelsing, J., Baquero, A.F., Hecksher-Sørensen, J., Cowley, M.A., Dalbøge, L.S., Hansen, G., Grove, K.L., Pyke, C., Raun, K., et al. (2014). The arcuate nucleus mediates GLP-1 receptor agonist liraglutide-dependent weight loss. *J. Clin. Invest.* 124, 4473–4488. <https://doi.org/10.1172/JCI75276>.
  23. de Lartigue, G., Lur, G., Dimaline, R., Varro, A., Raybould, H., and Dockray, G.J. (2010). EGR1 is a target for cooperative interactions between cholecystokinin and leptin, and inhibition by ghrelin, in vagal afferent neurons. *Endocrinology* 151, 3589–3599. <https://doi.org/10.1210/en.2010-0106>.
  24. Haghighi, A., Melka, M.G., Bernard, M., Abrahamowicz, M., Leonard, G.T., Richer, L., Perron, M., Veillette, S., Xu, C.J., Greenwood, C.M.T., et al. (2014). Opioid receptor mu 1 gene, fat intake and obesity in adolescence. *Mol. Psychiatry* 19, 63–68. <https://doi.org/10.1038/mp.2012.179>.
  25. Farooqi, I.S., Keogh, J.M., Yeo, G.S.H., Lank, E.J., Cheetham, T., and O'Rahilly, S. (2003). Clinical spectrum of obesity and mutations in the melanocortin 4 receptor gene. *N. Engl. J. Med.* 348, 1085–1095. <https://doi.org/10.1056/NEJMoa022050>.
  26. Pontieri, F.E., Tanda, G., Orzi, F., and Di Chiara, G. (1996). Effects of nicotine on the nucleus accumbens and similarity to those of addictive drugs. *Nature* 382, 255–257. <https://doi.org/10.1038/382255a0>.
  27. Alhadeff, A.L., Rupprecht, L.E., and Hayes, M.R. (2012). GLP-1 neurons in the nucleus of the solitary tract project directly to the ventral tegmental area and nucleus accumbens to control for food intake. *Endocrinology* 153, 647–658. <https://doi.org/10.1210/en.2011-1443>.
  28. Mohebi, A., Pettibone, J.R., Hamid, A.A., Wong, J.M.T., Vinson, L.T., Patriarchi, T., Tian, L., Kennedy, R.T., and Berke, J.D. (2019). Dissociable dopamine dynamics for learning and motivation. *Nature* 570, 65–70. <https://doi.org/10.1038/s41586-019-1235-y>.
  29. Patriarchi, T., Cho, J.R., Merten, K., Howe, M.W., Marley, A., Xiong, W.H., Folk, R.W., Broussard, G.J., Liang, R., Jang, M.J., et al. (2018). Ultrafast neuronal imaging of dopamine dynamics with designed genetically encoded sensors. *Science* 360, eaat4422. <https://doi.org/10.1126/science.aat4422>.
  30. Egecioglu, E., Engel, J.A., and Jerlhag, E. (2013). The glucagon-like peptide 1 analogue Exendin-4 attenuates the nicotine-induced locomotor stimulation, accumbal dopamine release, conditioned place preference as well as the expression of locomotor sensitization in mice. *PLoS One* 8, e77284. <https://doi.org/10.1371/journal.pone.0077284>.
  31. Mameli-Engvall, M., Evrard, A., Pons, S., Maskos, U., Svensson, T.H., Changeux, J.P., and Faure, P. (2006). Hierarchical control of dopamine neuron-firing patterns by nicotinic receptors. *Neuron* 50, 911–921. <https://doi.org/10.1016/j.neuron.2006.05.007>.
  32. Maskos, U., Molles, B.E., Pons, S., Besson, M., Guiard, B.P., Guilloux, J.P., Evrard, A., Cazala, P., Cormier, A., Mameli-Engvall, M., et al. (2005). Nicotine reinforcement and cognition restored by targeted expression of nicotinic receptors. *Nature* 436, 103–107. <https://doi.org/10.1038/nature03694>.
  33. Willi, C., Bodenmann, P., Ghali, W.A., Faris, P.D., and Cornuz, J. (2007). Active smoking and the risk of type 2 diabetes: a systematic review and

- meta-analysis. *JAMA* 298, 2654–2664. <https://doi.org/10.1001/jama.298.22.2654>.
34. Duncan, A., Heyer, M.P., Ishikawa, M., Caligiuri, S.P.B., Liu, X.A., Chen, Z., Micioni Di Bonaventura, M.V., Elayouby, K.S., Ables, J.L., Howe, W.M., et al. (2019). Habenular TCF7L2 links nicotine addiction to diabetes. *Nature* 574, 372–377. <https://doi.org/10.1038/s41586-019-1653-x>.
  35. WHO (2022). World Health Organisation. <https://www.who.int/news-room/fact-sheets/detail/tobacco>.
  36. Jall, S., De Angelis, M., Lundsgaard, A.M., Fritzen, A.M., Nicolaisen, T.S., Klein, A.B., Novikoff, A., Sachs, S., Richter, E.A., Kiens, B., et al. (2020). Pharmacological targeting of alpha3beta4 nicotinic receptors improves peripheral insulin sensitivity in mice with diet-induced obesity. *Diabetologia* 63, 1236–1247. <https://doi.org/10.1007/s00125-020-05117-4>.
  37. Finan, B., Yang, B., Ottaway, N., Stemmer, K., Müller, T.D., Yi, C.X., Habegger, K., Schriever, S.C., García-Cáceres, C., Kabra, D.G., et al. (2012). Targeted estrogen delivery reverses the metabolic syndrome. *Nat. Med.* 18, 1847–1856. <https://doi.org/10.1038/nm.3009>.
  38. Décarie-Spain, L., Fiset, A., Zhu, Z., Yang, B., DiMarchi, R.D., Tschöp, M.H., Finan, B., Fulton, S., and Clemmensen, C. (2019). GLP-1/dexamethasone inhibits food reward without inducing mood and memory deficits in mice. *Neuropharmacology* 151, 55–63. <https://doi.org/10.1016/j.neuropharm.2019.03.035>.
  39. He, R., Finan, B., Mayer, J.P., and DiMarchi, R.D. (2019). Peptide conjugates with small molecules designed to enhance efficacy and safety. *Molecules* 24, 1855. <https://doi.org/10.3390/molecules24101855>.
  40. Sherman, M.M., Ungureanu, S., and Rey, J.A. (2016). Naltrexone/bupropion ER (contrave): newly approved treatment option for chronic weight management in obese adults. *P T.* 41, 164–172.
  41. Christensen, R., Kristensen, P.K., Bartels, E.M., Bliddal, H., and Astrup, A. (2007). Efficacy and safety of the weight-loss drug rimonabant: a meta-analysis of randomised trials. *Lancet* 370, 1706–1713. [https://doi.org/10.1016/S0140-6736\(07\)61721-8](https://doi.org/10.1016/S0140-6736(07)61721-8).
  42. Reichenbach, A., Clarke, R.E., Stark, R., Lockie, S.H., Mequinion, M., Dempsey, H., Rawlinson, S., Reed, F., Sepehrizadeh, T., DeVeer, M., et al. (2022). Metabolic sensing in AgRP neurons integrates homeostatic state with dopamine signalling in the striatum. *Elife* 11, e72668. <https://doi.org/10.7554/eLife.72668>.
  43. Mazzone, C.M., Liang-Guallpa, J., Li, C., Wolcott, N.S., Boone, M.H., Southern, M., Kobzar, N.P., Salgado, I.d.A., Reddy, D.M., Sun, F., et al. (2020). High-fat food biases hypothalamic and mesolimbic expression of consummatory drives. *Nat. Neurosci.* 23, 1253–1266. <https://doi.org/10.1038/s41593-020-0684-9>.
  44. Jørgensen, S.H., Ejdrup, A.L., Lycas, M.D., Posselt, L.P., Madsen, K.L., Tian, L., Dreyer, J.K., Herborg, F., Sørensen, A.T., and Gether, U. (2023). Behavioral encoding across timescales by region-specific dopamine dynamics. *Proc. Natl. Acad. Sci. USA* 120, e2215230120. <https://doi.org/10.1073/pnas.2215230120>.
  45. Xu, W., Orr-Urtreger, A., Nigro, F., Gelber, S., Sutcliffe, C.B., Armstrong, D., Patrick, J.W., Role, L.W., Beaudet, A.L., and De Biasi, M. (1999). Multi-organ autonomic dysfunction in mice lacking the beta2 and the beta4 subunits of neuronal nicotinic acetylcholine receptors. *J. Neurosci.* 19, 9298–9305. <https://doi.org/10.1523/JNEUROSCI.19-21-09298.1999>.
  46. Chalfoun, J., Majurski, M., Blattner, T., Bhadriraju, K., Keyrouz, W., Bajcsy, P., and Brady, M. (2017). MIST: accurate and scalable microscopy image stitching tool with stage modeling and error minimization. *Sci. Rep.* 7, 4988. <https://doi.org/10.1038/s41598-017-04567-y>.
  47. Renier, N., Adams, E.L., Kirst, C., Wu, Z., Azevedo, R., Kohl, J., Autry, A.E., Kadiri, L., Umadevi Venkataraju, K., Zhou, Y., et al. (2016). Mapping of brain activity by automated volume analysis of immediate early genes. *Cell* 165, 1789–1802. <https://doi.org/10.1016/j.cell.2016.05.007>.
  48. Renier, N., Wu, Z., Simon, D.J., Yang, J., Ariel, P., and Tessier-Lavigne, M. (2014). iDISCO: a simple, rapid method to immunolabel large tissue samples for volume imaging. *Cell* 159, 896–910. <https://doi.org/10.1016/j.cell.2014.10.010>.
  49. Hansen, H.H., Perens, J., Roostalu, U., Skytte, J.L., Salinas, C.G., Barkholt, P., Thorbek, D.D., Rigbolt, K.T.G., Vrang, N., Jelsing, J., and Hecksher-Sørensen, J. (2021). Whole-brain activation signatures of weight-lowering drugs. *Mol. Metab.* 47, 101171. <https://doi.org/10.1016/j.molmet.2021.101171>.
  50. Perens, J., Salinas, C.G., Skytte, J.L., Roostalu, U., Dahl, A.B., Dyrby, T.B., Wichern, F., Barkholt, P., Vrang, N., Jelsing, J., and Hecksher-Sørensen, J. (2021). An optimized mouse brain atlas for automated mapping and quantification of neuronal activity using iDISCO+ and light sheet fluorescence microscopy. *Neuroinformatics* 19, 433–446. <https://doi.org/10.1007/s12021-020-09490-8> (2021).
  51. Nobili, A., Latagliata, E.C., Viscomi, M.T., Cavallucci, V., Cutuli, D., Giacobuzzo, G., Krashia, P., Rizzo, F.R., Marino, R., Federici, M., et al. (2017). Dopamine neuronal loss contributes to memory and reward dysfunction in a model of Alzheimer’s disease. *Nat. Commun.* 8, 14727. <https://doi.org/10.1038/ncomms14727>.
  52. Qiu, J., Fang, Y., Rønnekleiv, O.K., and Kelly, M.J. (2010). Leptin excites proopiomelanocortin neurons via activation of TRPC channels. *J. Neurosci.* 30, 1560–1565. <https://doi.org/10.1523/JNEUROSCI.4816-09.2010>.
  53. Margolis, E.B., Lock, H., Hjelmstad, G.O., and Fields, H.L. (2006). The ventral tegmental area revisited: is there an electrophysiological marker for dopaminergic neurons? *J. Physiol.* 577, 907–924. <https://doi.org/10.1113/jphysiol.2006.117069>.
  54. Kohlmeier, K.A., and Leonard, C.S. (2006). Transmitter modulation of spike-evoked calcium transients in arousal related neurons: muscarinic inhibition of SNX-482-sensitive calcium influx. *Eur. J. Neurosci.* 23, 1151–1162. <https://doi.org/10.1111/j.1460-9568.2006.04640.x>.

## STAR★METHODS

### KEY RESOURCES TABLE

REAGENT or RESOURCE	SOURCE	IDENTIFIER
<b>Antibodies</b>		
Rabbit anti-mouse UCP-1 primary antibody	Alpha Diagnostics	CAT# #UCP11-A
Biotinylated goat anti-mouse IgG secondary antibody	Vector Laboratories	CAT# #BA-1000
Rabbit anti c-Fos antibody	Cell Signaling Technologies	CAT# 2250
Donkey anti rabbit Cy-5 antibody	Jackson ImmunoResearch	CAT# 711-175-152
Anti-GFP primary antibody	Abcam	CAT# ab13970
Goat anti-chicken IgY H&L (Alexa Fluor® 488)	Abcam	CAT# ab150173
POMC (27–52) (Porcine) primary antibody	Phoenix Pharmaceuticals	CAT# H-029-30
Donkey anti-rabbit IgG (H + L) (Alexa Fluor™ 488)	ThermoFischer Scientific	CAT# A21206
<b>Biological samples</b>		
Mouse plasma samples (C57BL/6J)	In house, UCPH	N/A
Mouse tissue samples (C57BL/6J)	In house, UCPH	N/A
Goat serum	Sigma-Aldrich	CAT# G9023
Coronal brain slices	In house, UCPH	N/A
<b>Bacterial and virus strains</b>		
AAV9-hSyn-dLight1.3b-WPREpA	In house, UCPH <sup>44</sup>	Patriarchi et al. 2018 <sup>29</sup>
<b>Chemicals, peptides, and recombinant proteins</b>		
High-fat, high-sugar rodent diet (58 kcal% fat, 25.5 kcal% carbohydrate, 16.4 kcal% protein)	Research Diets	CAT# D12331i
Rodent chow diet	Brogaarden	CAT# V1534-300
(–)-nicotine hydrogen tartrate salt dihydrate	Sigma-Aldrich	CAT# 1463304
Victoza (liraglutide) pen, 6 mg mL <sup>-1</sup>	Novo Nordisk A/S	N/A
NBQX disodium salt hydrate	Sigma-Aldrich	CAT# N183
Exendin 9-39	Novo Nordisk A/S	N/A
Paraformaldehyde (PFA)	Sigma-Aldrich	CAT# 158127
Phosphate buffered saline (PBS)	Substrate department, UCPH	N/A
Hematoxylin solution, Mayer's	BioOptica	CAT# 05–06002/L
Eosin Y	BioOptica	CAT# 05–10007/L
Sodium citrate dihydrate	Sigma-Aldrich	CAT# W302600
Hypnorm-Dormicum	Roche	N/A
Heparinized PBS (15.000 U/L)	Leo Pharma	N/A
10% neutral buffered formalin	CellPath	CAT# BAF-0010-25A
Sodium Azide	Sigma-Aldrich	CAT# 438456
RNAlater	Sigma-Aldrich	CAT# #R0901
Lidocaine	Supelco	N/A
Rimadyl	Pfizer	N/A
Isoflurane	Baxter	N/A
Tetric EvoFlow dental cement	Ivoclar Vivadent	N/A
Optibond FL sealing primer	Kerr	N/A
Optibond FL Adhesive	Kerr	N/A
Bovine serum albumin (BSA)	Sigma-Aldrich	CAT# A7030
Triton™ X-100	Sigma-Aldrich	CAT# 11332481001
Prolong™ gold antifade mounting medium	ThermoFischer Scientific	CAT#P36934
Artificial cerebrospinal fluid (ACSF)	Tocris	CAT# 3525

(Continued on next page)

REAGENT or RESOURCE	SOURCE	IDENTIFIER
Bis-Fura	Molecular Probes	CAT# F6774
Alexa 594	Molecular Probes	CAT# A37572
DAPI	Sigma-Aldrich	CAT# D9542
<b>Critical commercial assays</b>		
ABC peroxidase staining kit	ThermoFischer Scientific	CAT# #32020
Mouse/rat insulin kit	Meso Scale Discovery	CAT# L452BZA-1
RNeasy mini kit	Qiagen	CAT# 74106
TruSeq RNA Library Prep Kit v2	Illumina	CAT# RS-122-2001/CAT# RS-122-2002
Superscript III reverse transcriptase	ThermoFischer Scientific	CAT# 12574026
AMPure XP Reagent	Beckman Coulter	CAT# A63880
<b>Deposited data</b>		
RNA sequencing data	This paper	GEO: GSE229789
RNA sequencing ARC	This paper	Zenodo: <a href="https://doi.org/10.5281/zenodo.7823574">https://doi.org/10.5281/zenodo.7823574</a>
Fiber photometry data and scripts	This paper	Zenodo: <a href="https://doi.org/10.5281/zenodo.7819630">https://doi.org/10.5281/zenodo.7819630</a>
<b>Experimental models: Organisms/strains</b>		
C57BL/6J mice	Janvier laboratories	C57BL/6J mice
NMRI mice	Charles river laboratories	NMRI mice
Global CHRNb4 KO	Xu et al. 1999 <sup>45</sup>	<i>Chrn4</i> KO mice
<b>Software and algorithms</b>		
ImageJ	ImageJ	<a href="https://imagej.nih.gov">https://imagej.nih.gov</a>
Noldus EthoVision XT 14™	Noldus	<a href="https://noldus.com">https://noldus.com</a>
GraphPad Prism 9.4.1	GraphPad	<a href="https://graphpad.com">https://graphpad.com</a>
TILL-VISION	Till Photonics	N/A
MiniAnalysis	Synaptosoft	<a href="https://synaptosoft.com">https://synaptosoft.com</a>
ImageJ MIST	Chalfoun et al. 2017 <sup>46</sup>	<a href="https://imagej.nih.gov">https://imagej.nih.gov</a>
MATLAB2019b	MathWorks	<a href="https://mathworks.com">https://mathworks.com</a>
Python 3.6.10	Python	<a href="https://python.org">https://python.org</a>
SciPy v1.5.2	Python plugin	N/A
Numpy v1.18.1	Python plugin	N/A
Pulse 9.0	HEKA	<a href="https://heka.com">https://heka.com</a>
AxoScope 10.2	Molecular Devices Corporation	<a href="https://moleculardevices.com">https://moleculardevices.com</a>
Axiovision 4.6	Zeiss	<a href="https://zeiss.com">https://zeiss.com</a>
Clampfit 10.3	Molecular Devices Corporation	<a href="https://moleculardevices.com">https://moleculardevices.com</a>
<b>Other</b>		
EchoMRI™-4in1 body composition analyzer	EchoMRI	N/A
10x light sheet microscope	Bruker	N/A
Contour XT glucometer	Bayer	N/A
Logitech C920 pro camera (1080x1080 pixels)	Logitech software	N/A
Leica cryostat	Leica biosystems	CM 3050S
HiSeq 1500 System	Illumina	N/A
Fragment analyzer	Agilent Technologies	N/A
NovaSeq 6000	Illumina	N/A
Guide-cannula	Invivo1	CAT#C235GS-5-1.2/SPC
Internal-cannula	Invivo1	CAT#C235IS-5/SPC
Fiber optic cannula	Doric Lenses	CAT#D148-0388
Neurophotometrics FP3001 system	Neurophotometrics	N/A

(Continued on next page)

**Continued**

REAGENT or RESOURCE	SOURCE	IDENTIFIER
Branching fiber optic patch cord	Doric Lenses	N/A
Bronze mating sleeve	Thorlabs	CAT#ADAL4-5
Epifluorescent microscope	FEI CorrSight, UCPH	N/A
Leica vibratome	Leica biosystems	VT1200S
Microscope recording chamber	Warner Instruments	RC27
40x water immersion objective	Olympus	NA 0.8
Sutter P-97 horizontal puller	Sutter Instruments	N/A
Patch clamp EPC9 amplifier	HEKA	N/A
Axon Digidata 1440A digitizer	Molecular Devices Corporation	N/A
12-bit CCD fluorescent camera	PCO Instruments	Sensicam
Emission filter of 510 nm	Till Photonics	Chroma Fura-2 cube filter sets
Axioskop 2	Zeiss	N/A
Axiocam MRM	Zeiss	N/A

**RESOURCE AVAILABILITY**

**Lead contact**

Further information and requests for resources should be directed to and will be fulfilled by the lead contact, Christoffer Clemmensen ([chc@sund.ku.dk](mailto:chc@sund.ku.dk)).

**Materials availability**

The study did not generate new unique reagents.

**Data and code availability**

- RNA-seq data have been deposited at GEO and are publicly available as of the date of publication. Accession numbers are listed in the [key resources table](#).
- All original code has been deposited at Zenodo and is publicly available as of the date of publication. DOIs are listed in the [key resources table](#).
- Any additional information required to reanalyze the data reported in this paper is available from the [lead contact](#) upon request.

**EXPERIMENTAL MODELS AND SUBJECT DETAILS**

**Animals**

All *in vivo* experiments were conducted at the University of Copenhagen, Denmark, according to internationally accepted principles for animal care and under approval from the Danish Animal Experiments Inspectorate, Danish Ministry of Food, Agriculture and Fisheries (permit number: 2018-15-0201-01457). The mice were single- or double-housed in an enriched and temperature-controlled environment (21–23°C) maintained on a 12-h light-dark cycle (light: 6:00 am - 6:00 pm; dark: 6:00 pm–6:00 am) with *ad libitum* access to food and drinking water, unless otherwise specified. All *in vivo* experiments were conducted using male mice. Unless otherwise specified, experiments were conducted using C57Bl/6J mice (Janvier, FR) kept on a high-fat, high sugar (HFHS) diet (58 kcal% fat, 25.5 kcal% carbohydrate, 16.4 kcal% protein, #D12331i, Research Diets, New Brunswick, NJ, US) from 8 weeks of age. Mice were maintained on *ad libitum* HFHS diet for a minimum of 16 weeks, and all pharmacological studies were conducted on mice with an average body weight of >45g. Electrophysiology was conducted using male NMRI mice (Charles River Laboratories, Germany) at 5 to 7 weeks of age. Aversion studies using an open field test was carried out using lean wildtype C57BL/6J mice with *ad libitum* access to tap water and standard chow diet (Altromin 1324, Brogaarden, DK). Global *Chrb4* ( $\beta_4$ ) KO and WT mice on a C57BL/6J background were used for studying the role of  $\alpha_3\beta_4$  nAChRs.<sup>16,45</sup>

**METHOD DETAILS**

**Pharmacology**

Experimental compounds were purchased from commercial sources in highest possible purity (>95%). Compounds were acquired as (–)-nicotine hydrogen tartrate salt dihydrate (CAT# 1463304, Sigma-Aldrich, DK), liraglutide (Victoza, Novo Nordisk A/S, DK), Exendin 9-39 (Novo Nordisk A/S, DK) and NBQX disodium salt hydrate (CAT# N183, Sigma-Aldrich, DK). Mice were randomized into

experimental groups on the first day the experiment. The compounds were formulated as stock solutions in sterile water ( $1 \text{ mg mL}^{-1}$ ) and diluted to the dose levels specified for each study using isotonic saline. All compounds were administered as once-daily subcutaneous injections (between 3pm and 6pm) at a volume of  $5 \mu\text{L g}^{-1}$  of body weight based on measurements of body weight immediately prior to injection and with concomitant measurement of food intake, unless otherwise specified. Vehicle groups were treated with isotonic saline at a volume of  $5 \mu\text{L g}^{-1}$  of body weight.

### Pair-feeding

Single- or double-housed DIO mice were randomized into experimental groups receiving once-daily subcutaneous administrations of vehicle (isotonic saline) or co-administration of nicotine ( $1 \text{ mg kg}^{-1}$ ) and liraglutide ( $10 \text{ nmol kg}^{-1}$ ). The food intake of the pair-fed group was delayed one day to match the food intake of the co-administration treated group's food intake from the previous day. Experimental compounds were administered at volume of  $5 \mu\text{L g}^{-1}$  of body weight based on measurement of body weight immediately prior to injection and with concomitant measurement of food intake.

### Body composition measurement

Body composition measures were conducted 3 days prior to study start and, on the day, following the final injection using an EchoMRI<sup>TM</sup>-4in1 body composition analyzer (EchoMRI, US).

### Tissue harvest and processing

Mice were euthanized by decapitation for collection of plasma and tissues. Plasma was collected immediately after decapitation in EDTA-coated microvette tubes and stored at  $-20^\circ\text{C}$  until further processing. Tissues were collected by dissection, snap-frozen on dry ice and stored at  $-80^\circ\text{C}$  until further processing. Liver tissue was drop-fixed in 4% PFA in PBS buffer for at least 24 h and stored in PBS + 0.1% PFA at  $4^\circ\text{C}$  until processed.

### Pathohistological analyses

Tissue samples of 5–10 mm were dehydrated in ethanol and xylene and embedded in paraffin. Slices of  $3 \mu\text{m}$  thickness were prepared, deparaffinized, rehydrated and stained with Mayer's Hematoxylin (CAT# 05-06002/L, BioOptica, IN) and Eosin Y (CAT# 05-10007/L, BioOptica, IN). Histological images were acquired using 10x light microscopy ( $1360 \times 1024$  pixels) and quantified using ImageJ software. Data is reported as the mean of three independent H&E-stained sections per mouse.

For UCP-1 immunoreactivity, brown-adipose tissue embedded in paraffin was treated with 10 nM sodium citrate, blocked with goat-serum and stained employing rabbit anti-mouse UCP-1 primary antibody (1:400, UCP11-A, Alpha Diagnostics, US). Signal detection was achieved using biotinylated goat anti-rabbit IgG secondary antibody (1:200, BA-1000, US) and ABC peroxidase staining kit (CAT# 32020, Thermofischer Scientific, DK).

### Blood glucose and insulin measures

Prior to tissue isolation acute blood glucose was measured from tail blood using a glucometer (Contour XT, Bayer, DK). Blood samples for insulin measures were collected immediately after decapitation and cooled to  $4^\circ\text{C}$ . Samples were centrifuged for 10 min at  $4^\circ\text{C}$ , 3000rcf. The commercially available mouse/rat insulin kit was utilized according to manufacturer's protocol to determine plasma insulin levels (CAT# L452BZA-1, Meso Scale Discovery, DE).

### Open field test

General locomotor activity was evaluated using an open field test. Mice were acclimatized for 7 days in the procedure room prior to study start. Mice were placed one in each of four  $50 \times 50 \times 50 \text{ cm}$  chambers immediately after s.c. administration of compounds (vehicle (isotonic saline),  $1 \text{ mg kg}^{-1}$  nicotine,  $10 \text{ nmol kg}^{-1}$  liraglutide, or co-administration of  $1 \text{ mg kg}^{-1}$  nicotine and  $10 \text{ nmol kg}^{-1}$  liraglutide) and their locomotor activity recorded over 10 min using a ceiling-mounted Logitech C920 Pro camera ( $1080 \times 1080$  pixels, 30fps, Logitech software, DK). Mice were divided into four groups ( $n = 8$ ) and their movement recorded for 10 min. Each run was conducted with one mouse from each treatment group and with run-to-run alternation so that treatments were equally distributed across all chambers. Movement traces and quantification of locomotor activity (velocity and distance traveled) were obtained using Noldus EthoVision XT 14<sup>TM</sup> software (Noldus, NL).

### Unbiased whole-brain c-Fos imaging

Double-housed DIO mice were randomized and treated with sham injections for 5 days prior to study start. At study start, mice were treated with a single s.c. injection of the experimental compounds (vehicle,  $1 \text{ mg kg}^{-1}$  nicotine,  $10 \text{ nmol kg}^{-1}$  liraglutide, or co-administration of  $1 \text{ mg kg}^{-1}$  nicotine and  $10 \text{ nmol kg}^{-1}$  liraglutide) and anaesthetized after 2 h using a mixture of Hypnorm-Dormicum (fentanyl at  $0.315 \text{ mg mL}^{-1}$ ; fluanisone at  $10 \text{ mg mL}^{-1}$  and midazolam at  $5 \text{ mg mL}^{-1}$ , Roche, CH). The mice were intracardially perfused with heparinized phosphate buffered saline ( $15,000 \text{ IU/L}$ , Leo Pharma, DK) and 10% neutral buffered formalin (NBF) (CAT# BAF-0010-25A, CellPath, DK), their brains harvested and drop-fixed in NBF overnight. The next day, brains were washed using phosphate buffered saline ( $3 \times 30 \text{ min}$ ) and stored in phosphate buffered saline containing 0.02% Sodium Azide (CAT# 438456, Sigma-Aldrich, DK) until further processed. Brain samples Tissue processing and quantification of c-Fos was conducted according to iDISCO+ protocols.<sup>47–50</sup>

### Brain region abbreviations

NAC, Nucleus accumbens; PVH, Paraventricular hypothalamic nucleus; DMH, Dorsomedial nucleus of the hypothalamus; ARC, Arcuate nucleus of the hypothalamus; LHA, Lateral hypothalamic area; CEA, Central amygdalar nucleus; SNc, Substantia nigra, compact part; VTA, Ventral tegmental area; PB, Parabrachial nucleus; NTS, Nucleus of the solitary tract; DMX, Dorsal motor nucleus of the vagus nerve; AP, Area postrema; PGRNI, Paragigantocellular reticular nucleus, lateral part; SCs, Superior colliculus sensory related; MD, Mediodorsal nucleus of thalamus; PVT, Paraventricular nucleus of the thalamus; RR, Midbrain reticular nucleus, retro-rubral area; PSTN, Parasubthalamic nucleus; PT, Parataenial nucleus; SUT, Supratrigeminal nucleus; RE, Nucleus of reuniens; SPA, Subparafascicular area; BST, Bed nuclei of the stria terminalis; BMA, Basomedial amygdalar nucleus; CP, Caudoputamen; LRNm, Lateral reticular nucleus, magnocellular part; BLAa, Basolateral amygdalar nucleus, anterior part; PIR, Piriform area; PVHd, Paraventricular hypothalamic nucleus, descending division; COA, Cortical amygdalar area; PMd, Dorsal premammillary area; PT, Parataenial nucleus; SCm, Superior colliculus, motor related; MEA, Medial amygdalar nucleus; TU, Tuberal nucleus; PAA, Piriform-amygdalar area; VISpl, Posterolateral visual area; VMH, Ventromedial hypothalamic nucleus; IG, Induseum griseum; TRN, Tegmental reticular nucleus; IA, Intercalated amygdalar nucleus.

### RNA sequencing

DIO mice were randomized, and sham injected for 7 days prior to study start. Mice were treated with daily s.c. injections of experimental compounds for 3 days (vehicle (isotonic saline), 1 mg kg<sup>-1</sup> nicotine, 10 nmol kg<sup>-1</sup> liraglutide, or co-administration of 1 mg kg<sup>-1</sup> nicotine and 10 nmol kg<sup>-1</sup> liraglutide). At day 3, the mice were decapitated 3 h after administration, their brains harvested and snap frozen on dry ice. The brains were subsequently cut into 250 μm on a cryostat and stored in RNAlater (CAT# R0901, Sigma-Aldrich, DK) at 4°C. Regions of interest were microdissected using laser capture microscopy and snap-frozen using dry ice. Total RNA was isolated using RNeasy mini kit (CAT# 74106, Qiagen, US) according to manufacturer's protocol. Messenger RNA sequencing libraries were prepared using the Illumina TruSeq Stranded mRNA protocol (CAT# RS-122-2001, Illumina, US). Poly-A containing mRNAs were purified by poly-T attached magnetic beads, fragmented, and cDNA was synthesized using SuperScript III Reverse Transcriptase (CAT# 12574026, Thermofisher Scientific, DK). cDNA was adenylated to prime for adapter ligation and after clean-up, using AMPure XP beads (CAT# A63881, Beckman coulter, DK), DNA fragments were amplified using PCR followed by a final clean-up. Libraries were quality-controlled using a fragment analyzer (Agilent Technologies, DK) and subjected to 52-bp paired-end sequencing on a NovaSeq 6000 (Illumina, US). A total of 3.8 billion reads were generated.

### Differential expression testing

The R package DESeq2 (v. 1.30.1) was used to identify differentially expressed genes. *p* values were adjusted for multiple testing using the Benjamini-Hochberg (BH) *post hoc* method. *Gene Ontology analysis*: The R package gprofiler2 (v.0.2.0) was used to identify enriched GO terms (categories: molecular function, biological process, cellular component, KEGG pathways, REACTOME pathways). The gene set enrichment analysis was carried out with the parameters 'exclude\_jea' set to true and 'correction method' set to BH.

### ARC and VTA cannulations

Cannulation of the ARC VTA in DIO mice (Guide-cannula: Bilateral, short-pedestal 5mm, gauge 26, center to center distance 1.2, cut 4.4mm below pedestal, CAT# C235GS-5-1.2/SPC, invivo1, DE) were performed under isoflurane anesthesia, using the following stereotaxic coordinates: ARC 1.75 mm AP; 5.7 mm DV; 0.3 mm ML and; VTA -3.2 mm AP; -4.4mm DV; +/-0.6 mm ML. Animals were treated with lidocaine on the day of surgery and Rimadyl (5 mg kg<sup>-1</sup>, Pfizer, US) postoperatively for 3 days and were allowed to recover for at least 7 days before pharmacological testing. NBQX (Dose: 0.4 μg per mouse) and Ex9-39 (10 μg per mouse) were dissolved in sterile water and infused through an internal-cannula (Internal-cannula: 33GA DBL, FIT 5MM PED GDE, FIT 4.4MM C235GS-5-1.2 W 0.2MM, CAT# C235IS-5/SPC, invivo1, DE) in a volume of 1 μL pr. side at a rate of 0.4 μL/min. The probe was left in for 2 min before extraction. Mice were treated with s.c. administration of experimental compounds 20 min after infusion (vehicle (isotonic saline) or co-administration of 1 mg kg<sup>-1</sup> nicotine and 10 nmol kg<sup>-1</sup> liraglutide), and food intake and body weight were monitored over 24 h. A within-subject design with counter-balanced treatment presentation was used with 7 days wash-out period in between. After the experiment brains were harvested and snap frozen on dry ice. Brains were subsequently cut on a cryostat to control for correct probe placement.

### Adeno-associated viral (AAV) vector infusion and fiber optic cannula implantation

AAV vector infusions were performed under isoflurane anesthesia as described for VTA cannulations. 300 nL AAV9-hSyn-dlight1.3b-WPREpA was injected into the Nucleus Accumbens using the following coordinates measured from Bregma: 1.54 mm AP, -4.30 mm DV, -0.80 mm ML at 100 nL min<sup>-1</sup> through a pulled glass needle. Additionally, 100 nL was injected 100 μm above and 100 μm below these coordinates. The needle was left in place for 5 min after infusion. A fiber optic cannula (200 μm fiber diameter, Numeric Aperture 0.37, 1.25 mm metal ferrule, Doric Lenses) was implanted with the fiber tip at coordinates 1.54 mm AP, -4.30 mm DV, -0.80 mm ML, and attached to the skull using light curing Tetric EvoFlow dental cement (Ivoclar Vivadent, LI) on top of a base of Optibond FL sealing primer (Kerr, CH) and Optibond FL Adhesive (Kerr, CH) which was applied before drilling and viral infusion commenced.

### **In vivo dopamine release recordings**

Fiber photometry recordings were performed using a Neurophotometrics FP3001 system (Neurophotometrics, US). The system was connected to pre-implanted optic cannulas using a branching fiber optic patch cord (200  $\mu\text{m}$ , 0.37 NA, Doric Lenses, CA) and a bronze mating sleeve (ADAL 4–5, Thorlabs, US). Fluorescence was measured from the 470 nm and 415 nm channel at 40 Hz (20 Hz pr. channel). Light power output was measured using a light power meter (PM100D + S130C 400–1100 nm sensor, Thorlabs, US) at the tip of the patch cord with constant illumination and set to  $\sim 25 \mu\text{W}$  for the 470 nm channel and  $\sim 18 \mu\text{W}$  for the 415 nm channel. These power levels were found to yield similar absolute fluorescence levels of the 470 and 415 nm channels. A technical background was first measured in black light-impermeable caps, then the mice were connected for recording and placed in an open field arena and allowed to habituate for 60 min in the chamber. Hereafter, a subcutaneous vehicle injection was given and 30 min later the experimental compound (vehicle (isotonic saline), 1 mg  $\text{kg}^{-1}$  nicotine, 10 nmol  $\text{kg}^{-1}$  liraglutide, or co-administration of 1 mg  $\text{kg}^{-1}$  nicotine and 10 nmol  $\text{kg}^{-1}$  liraglutide) was subcutaneously injected. Mice were subjected to three trials with the different experimental compounds with a 4-week wash-out period between test days and data were pooled from all trials. Mice were randomly assigned to test groups and the experimenter was blinded to the treatments. After the experiment mice were terminated, and brains were harvested and fixed in 4% PFA for 24 h and subsequently in 30% sucrose in PBS for 48 h before being frozen on crushed dry ice. Hereafter, the brains were cut in 40  $\mu\text{m}$  sections on a cryostat for verification of proper probe placement. To visualize dLight1.3b expression brain slices were stained using an anti-GFP antibody (1:1000, CAT# ab13970, Abcam, UK).

Slices were washed in PBS 3 times 5 min and then pre-incubated for 30 min in 5% goat serum, 1% BSA and 0.3% Triton<sup>TM</sup> X-100 in PBS at room temperature. Subsequently, slices were incubated overnight in an identical solution with the primary antibody added. Slices were then washed for  $3 \times 5$  minutes in 0.25% BSA and 0.1% Triton<sup>TM</sup> X-100 in PBS and hereafter incubated for 60 min in an identical solution containing the secondary antibody (Alexa 488, goat- $\alpha$ -chicken, Ab150173, 1:400). Slices were mounted on glass slides and allowed to air-dry and then covered with a coverslip using prolong<sup>TM</sup> gold antifade mounting medium (CAT# P36934ThermoFisher Scientific, DK). Probe locations were verified visually using an epifluorescent microscope (DM IL LED, Leica biosystems, DE) and representative images were acquired on a spinning disk confocal microscope (FEI CorrSight, Core Facility for Integrated Microscopy, University of Copenhagen). Images were stitched using the ImageJ plugin MIST using the linear stitching method.

### **Analysis of fiber photometry data**

Fiber photometry traces from dLight1.3b recordings were normalized to  $dF/F_0$  from a 20 min window prior to drug administration by subtracting the isosbestic 415 nm channel from the 470 nm signal channel, followed by division with the 415 nm channel. Differential photobleaching of the two channels was corrected for by linear fit to the  $dF/F_0$  before pharmacological intervention and applied across the entire series. The preprocessing was done in MATLAB 2019b and the postprocessing analysis in Python 3.6.10 (Python, US) using SciPy v1.5.2 and Numpy v1.18.1.

## **Electrophysiology**

### **Acute brain slice preparation**

Mice were decapitated following deep anesthesia with isoflurane (Baxter, DE). The brain was gently removed and immersed immediately into ice-cold artificial cerebrospinal fluid (ACSF) containing in mM: NaCl 124; KCl 5;  $\text{Na}_2\text{HPO}_4$  1.12;  $\text{CaCl}_2 \cdot 2\text{H}_2\text{O}$  2.7;  $\text{MgSO}_4$  (anhydrous) 1.12; Dextrose 10;  $\text{NaHCO}_3$  26; saturated with carbogen gas (5%  $\text{CO}_2$  + 95%  $\text{O}_2$ ) (CAT# 3525, Tocris, UK). Coronal brain slices (250  $\mu\text{m}$ ) containing the VTA and ARC nuclei were prepared using a Leica vibratome (VT 1200S, Leica biosystems, DE).<sup>51,52</sup> Following slicing, tissue was incubated in carbogen saturated ACSF for fifteen minutes at 37°C, and equilibrated for one hour at room temperature, before transferred to a microscope attached recording chamber (RC27, Warner Instruments, US) under continuous perfusion with ACSF at a flow rate of 1  $\text{mL min}^{-1}$  at ambient temperature.

### **Drug application**

For electrophysiology and calcium imaging experiments with brain slices containing the VTA and ARC, GLP-1R agonist (liraglutide 100 nM, Novo Nordisk A/S, DK) was bath applied, and (–)-nicotine hydrogen tartrate salt hydrate 10  $\mu\text{M}$  (CAT# 1463304, Sigma-Aldrich, DK) was locally applied to VTA or ARC neurons using a picospritzer (duration: 100 ms; pressure: 20 PSI).

### **Electrophysiology**

Whole-cell patch-clamp recordings were performed on VTA or ARC neurons visualized with a 40 $\times$  water immersion objective (NA 0.8, Olympus, JP). Patch pipette electrodes of thin wall borosilicate glass were produced using a Sutter P-97 horizontal puller (Sutter Instruments, US), and once filled with internal solution (containing in mM: K gluconate 144; KCl 2; HEPES 10; EDTA (tetraacetic acid) 0.2; Mg-ATP 5 and Na-GTP 0.3), exhibited resistances between 6 and 8  $\text{m}\Omega$ . High resistance seals ( $>1 \text{ m}\Omega$ ) were established between the patch pipette and the cell membrane via a patch clamp EPC9 amplifier (EPC9, HEKA, DE) in voltage clamp mode guided by Pulse (version 9.0, HEKA, DE). After that time, seals were broken by membrane rupture, and a holding current sufficient to maintain, or clamp, the cell at a voltage of  $-60 \text{ mV}$  was applied. Recordings of currents were sampled at a rate of 10 kHz using AxoScope (version 10.2, Molecular Devices Corporation, US) and an Axon Digidata 1440A digitizer (Molecular Devices Corporation, US). Recordings were discarded if the current necessary to hold the cell at  $-60 \text{ mV}$  exceeded 50 pA. For calcium imaging recordings, EGTA in the patch solution was substituted with 25  $\mu\text{M}$  of Fura-2 (Molecular Probes, US). Electrophysiologically, dopaminergic neurons in the VTA have been typically characterized by the presence of the hyperpolarization-activated current (I<sub>h</sub>).<sup>53</sup> Accordingly, to examine presence of this current, VTA neurons were clamped from the holding voltage of  $-60 \text{ mV}$  to more negative voltages in 8 successive

steps, in  $-10$  mV increments. Presence of Ih current was confirmed when a “sag” back of the membrane voltage to a more depolarized voltage was observed at the end of the step at the more hyperpolarized potentials. To identify the phenotype of the recorded neuron in the ARC, Alexa 594 ( $25 \mu\text{M}$ , Molecular Probes, US) was included in the intrapipette solution, which allowed conducting post hoc immunohistochemistry in order to detect presence or absence of POMC in the recorded cell.

### Calcium imaging

Elicitation of changes in intracellular calcium were examined using single-cell fluorescent imaging. Accordingly, Fura-2 was allowed to passively diffuse into the patched neuron from the EGTA-free intrapipette solution during the first 10 min following membrane rupture.<sup>54</sup> Fluorescent emissions from the target neuron were visualized and delineated with a region of interest (ROIs). To detect changes in Fura-2 fluorescence emission, a cooled, 12-bit CCD fluorescent camera (Sensicam, PCO Instruments, DE) with Xenon illumination was used. TILL-VISION software (Till Photonics, DE) controlled the camera and shutter. Fura-2 is a ratiometric dye with an increase (340 nm) and decrease (380 nm) of fluorescence emission when calcium is bound. Accordingly, we used excitation wavelengths of 340 nm and 380 nm from a PolyChrome V, and an emission filter of 510 nm (Chroma Fura-2 cube filter sets, Till Photonics, DE). An exposure time of 10 ms and an acquisition rate of 0.25–0.5 s were utilized. Images were binned at  $2 \times 2$ . Fluorescence values were averaged across the ROI, and, following subtraction of auto fluorescence as determined from imaging in a region devoid of filled cellular processes, were ratioed in a dimensionless value of  $F = F_{340}/F_{380}$ . Changes are reported as  $\Delta F/F$  (DF/F), which reflects subtraction of the average of ten frames taken at the maximum fluorescence change during the drug effect from the average fluorescence of 10 frames before drug application (baseline fluorescence, F), divided by F. DF/F data are presented in % to reflect the relative change from F, which is set at zero. Ascending deviations in the kinetics of % DF/F indicate increases in intracellular calcium, and it was determined that a change equal to, or greater than 5% in this measure would be sufficiently large to distinguish from noise.

### POMC neurons immunohistochemistry

POMC cells were phenotypically characterized by *post hoc* immunohistochemistry. Accordingly, ARC brain slices were placed in 4% paraformaldehyde for at least 4 h, and then stored in 30% sucrose in PBS (pH 7.4, Gibco, DK) for a minimum of 24 h. Slices were resectioned to a  $40 \mu\text{m}$  thickness on a cryostat (CM 3050S, Leica biosystems, DE). Later, these slices were rinsed 3 times for 5 min with Tris-Buffered Saline (TBS) and incubated in primary antibody (1:1000, CAT# H-029-30, Phoenix Pharmaceuticals, US) diluted in SUMI (gelatin and Trinton X-100 in TBS). After incubation overnight at  $4^\circ\text{C}$ , the slices were washed three times in TBS, and a fluorescent Alexa donkey anti-rabbit 488 secondary antibody incubated in SUMI during 2 h at room temperature (1:500, CAT# A21206, Thermofisher Scientific, DK). Slices were washed three times in TBS 10 min each; in the last wash TBS was supplemented with DAPI (1:10,000, CAT# D9542, Sigma-Aldrich, DK), dried at room temperature and mounted on slides. During patch clamp recordings of ARC cells, Alexa 594 was used to label the recorded cell, by passively diffusing from the patch pipette to the recorded cell where it remained. The recognition of the cell under study as a POMC-positive neuron was carried out by means of the co-visualization of the Alexa 594 signal, and that of the secondary antibody. Fluorescent signals were detected with appropriate Zeiss 59, fluorescent filter cube sets for the POMC antibody (358–463 nm) and Alexa 594 (472–578 nm), using a microscope (Axioskop 2, Zeiss, DE), which was fitted with a monochrome CCD digital camera (Axiocam MRM, Zeiss, DE). Images were collected using Axiovision 4.6 software (Zeiss, DE). Image analysis was performed using ImageJ software (National Institute of Health, MD). *Data analysis:* Amplitudes of the membrane inward currents generated by liraglutide, and nicotine were measured using Clampfit 10.3 (Molecular devices, US), and determined by the difference between the values of the current averaged 100 ms before and the maximum value of deflection of the current 100 ms after drug application. Spontaneous synaptic events (sEPSCs) were detected and analyzed using MiniAnalysis (Synatsoft, US) and data was binned in 30 s epochs. This epoch was used to evaluate the number of synaptic events, their amplitudes, and inter-event intervals.

### QUANTIFICATION AND STATISTICAL ANALYSES

Statistical analyses were performed using GraphPad Prism 9.0 (GraphPad, US). For comparison of multiple groups, one-way ANOVA or two-way repeated measures ANOVA were used. When ANOVA revealed a statistically significant interaction, Bonferroni post hoc multiple comparison analyses were applied. For comparison of two groups, unpaired two-tailed Students t-test were used. All data were evaluated for Gaussian distribution and equal variance with Shapiro-Hilk, Kolmogorov-Smirnov, and by visual inspection of the distribution residuals. Data from designated brain regions from the c-Fos 3D brain imaging study were analyzed by one-way ANOVA with Dunnet's post hoc multiple comparison test relative to vehicle, using a negative binomial generalized linear model to control for Gaussian distribution. No statistical methods were applied to predetermine sample size for *in vivo* pharmacology experiments. Data represent means  $\pm$  SEM. \* $p < 0.05$ , \*\* $p < 0.01$ , \*\*\* $p < 0.001$ , \*\*\*\* $p < 0.0001$ .

**Supplemental information**

**GLP-1 and nicotine combination therapy  
engages hypothalamic and mesolimbic  
pathways to reverse obesity**

**Sarah Falk, Jonas Petersen, Charlotte Svendsen, Cesar R. Romero-Leguizamón, Søren Heide Jørgensen, Nathalie Krauth, Mette Q. Ludwig, Kathrine Lundø, Urmas Roostalu, Grethe Skovbjerg, Duy Anh Gurskov Nielsen, Aske Lykke Ejdrup, Tune H. Pers, Oksana Dmytriyeva, Jacob Hecksher-Sørensen, Ulrik Gether, Kristi A. Kohlmeier, and Christoffer Clemmensen**

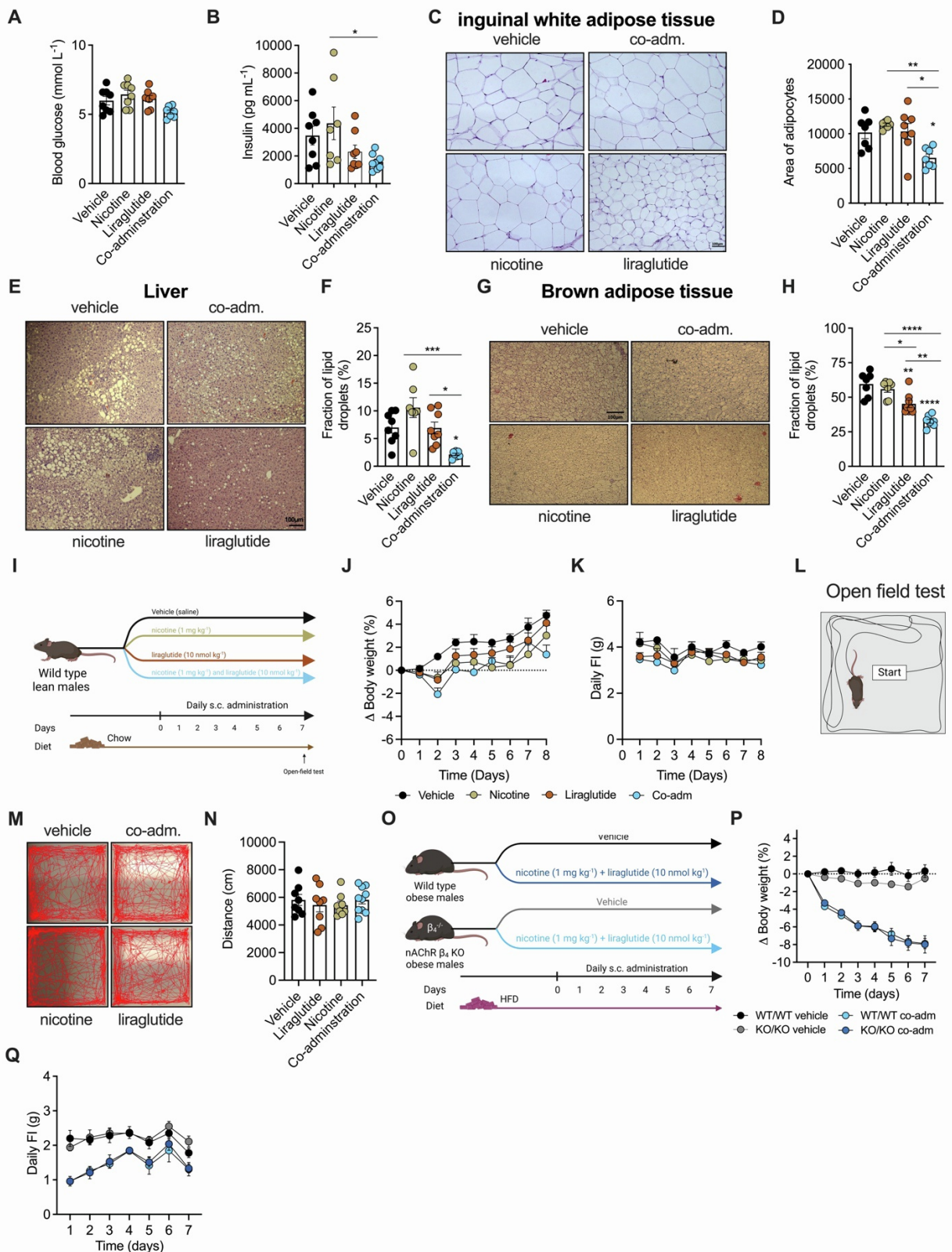


**Figure S1; Related to Figure 1. Liraglutide and nicotine co-administration in DIO, lean and *Chrnb4* KO mice.**

(A) Fasting blood glucose levels at day 16 from study in Figure 1A-F (n = 8, biological replicates). Data were analyzed by one-way ANOVA with Bonferroni multiple comparison test.

(B) Fasting plasma insulin levels from study in Figure 1A-F (n = 7-8, biological replicates). 1 mouse in nicotine group had non-determinable insulin plasma levels. Data were analyzed by one-way ANOVA with Bonferroni multiple comparison test, \*p < 0.05.

- (C) Representative images from H&E staining of inguinal white adipose tissue from study in Figures 1A-F. Scale bar = 100  $\mu$ m.
- (D) Quantification of area of adipocytes from study in Figure 1A-F (n = 5-8, biological replicates). Data was not collected from 3 samples in nicotine treatment group and 1 sample in nicotine and liraglutide co-treatment group due to poor tissue quality. Data were analyzed by one-way ANOVA with Bonferroni multiple comparison test, \*p < 0.05, \*\*p < 0.01.
- (E) Representative images from H&E staining of liver tissue from study in Figures 1A-F. Scale bar 100  $\mu$ m.
- (F) Quantification of hepatic lipid contents from study in Figure 1A-F (n = 7-8, biological replicates). Data was not collected from 1 sample in nicotine treatment group and 1 sample nicotine and liraglutide co-treatment group due to poor tissue quality. Data were analyzed by one-way ANOVA with Bonferroni multiple comparison test, \*p < 0.05, \*\*\*p < 0.001.
- (G) Representative images from H&E staining of brown adipose tissue from study in Figures 1A-F. Scale bar 100  $\mu$ m.
- (H) Quantification of lipid contents in brown adipose tissue from study in Figure 1A-F (n = 7-8, biological replicates). Data was not collected from 1 sample in vehicle treatment group and 1 sample nicotine treatment group due to poor tissue quality. Data were analyzed by one-way ANOVA with Bonferroni multiple comparison test, \*p < 0.05, \*\*p < 0.01, \*\*\*\*p < 0.0001.
- (I) Illustration of study in chow fed lean C57BL/6J male mice treated with once-daily subcutaneous (s.c.) injections of vehicle, liraglutide 10 nmol kg<sup>-1</sup>, nicotine 1 mg kg<sup>-1</sup> or co-administration of liraglutide 10 nmol kg<sup>-1</sup> and nicotine 1 mg kg<sup>-1</sup> for 7 days. Mice were subjected to an open field test the day after the final injection.
- (J) Change in body weight (n = 8-10, biological replicates). Data were analyzed by two-way RM ANOVA with Bonferroni multiple comparison test.
- (K) Daily food intake (n = 4-5, biological replicates). Data were analyzed by two-way RM ANOVA with Bonferroni multiple comparison test.
- (L) Illustration of open-field test conducted on mice in study outlined in panel I.
- (M) Representative traces from each treatment condition in the open field test.
- (N) Distance travelled during 10 minutes of open field test (n = 8-10, biological replicates). Data were analyzed by one-way ANOVA with Bonferroni multiple comparison test.
- (O) Illustration of study in high-fat diet (HFD)-induced obese C57BL/6J wildtype or  $\beta_4^{-/-}$  knockout male mice treated with once-daily s.c. injections of vehicle or co-administration of liraglutide 10 nmol kg<sup>-1</sup> and nicotine 1 mg kg<sup>-1</sup> for 7 days.
- (P) Change in body weight (n = 7-9, biological replicates). Data were analyzed by two-way RM ANOVA with Bonferroni multiple comparison test.
- (Q) Daily food intake (n = 5-6, biological replicates). Data were analyzed by two-way RM ANOVA with Bonferroni multiple comparison test.
- All data are reported as mean  $\pm$  SEM.

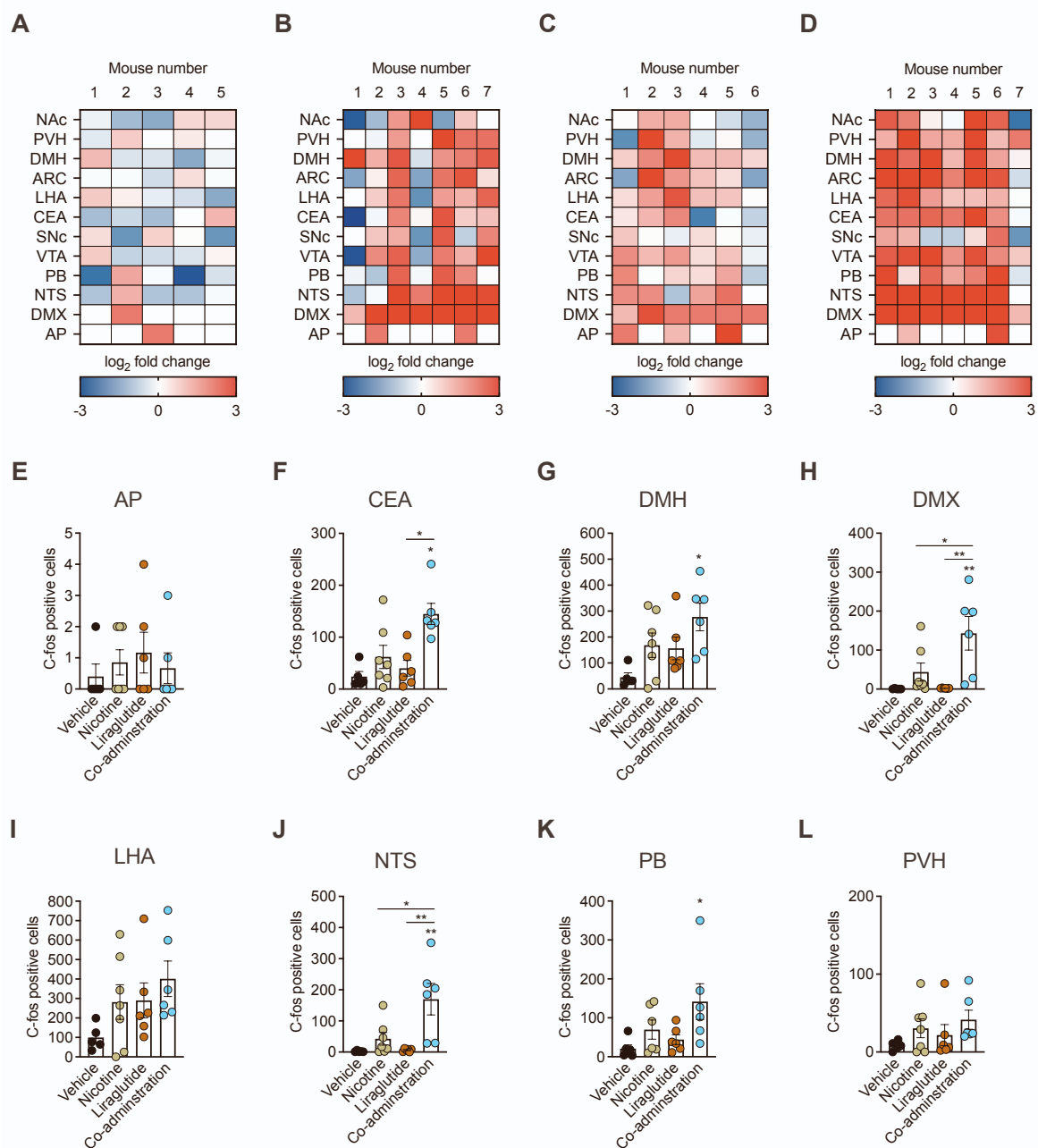


**Figure S2; Related to Figure 2. 3D whole-brain c-Fos assessment.**

(A) Heatmap showing  $\log_2$ fold changes in c-Fos expression in common brain areas involved in appetite regulation for each individual mouse in response to vehicle treatment and relative to vehicle. (n = 5, biological replicates).

(B) Heatmap showing  $\log_2$ fold changes in c-Fos expression in common brain areas involved in appetite regulation for each individual mouse in response to nicotine treatment and relative to vehicle. (n = 7, biological replicates).

(C) Heatmap showing  $\log_2$ fold changes in c-Fos expression in common brain areas involved in appetite regulation for each individual mouse in response to liraglutide treatment and relative to vehicle. (n = 6, biological replicates).

(D) Heatmap showing  $\log_2$ fold changes in c-Fos expression in common brain areas involved in appetite regulation for each individual mouse in response to co-administration treatment and relative to vehicle. (n = 7, biological replicates).

(E) Quantification of c-Fos positive cells in area postrema (n = 5-7, biological replicates). Data were analyzed by one-way ANOVA with Bonferroni multiple comparison test.

(F) Quantification of c-Fos positive cells in central amygdalar (n = 5-7, biological replicates). Data were analyzed by one-way ANOVA with Bonferroni multiple comparison test, \*p < 0.05.

(G) Quantification of c-Fos positive cells in dorsomedial nucleus of the hypothalamus (n = 5-7, biological replicates). Data were analyzed by one-way ANOVA with Bonferroni multiple comparison test, \*p < 0.05, \*\*p < 0.01.

(H) Quantification of c-Fos positive cells in dorsal motor nucleus of the vagus nerve (n = 5-7, biological replicates). Data were analyzed by one-way ANOVA with Bonferroni multiple comparison test, \*p < 0.05.

(I) Quantification of c-Fos positive cells in lateral hypothalamic area (n = 5-7, biological replicates). Data were analyzed by one-way ANOVA with Bonferroni multiple comparison test.

(J) Quantification of c-Fos positive cells in nucleus of the solitary tract (n = 5-7, biological replicates). Data were analyzed by one-way ANOVA with Bonferroni multiple comparison test, \*p < 0.05, \*\*p < 0.01.

(K) Quantification of c-Fos positive cells in parabrachial nucleus (n = 5-7, biological replicates). Data were analyzed by one-way ANOVA with Bonferroni multiple comparison test, \*p < 0.05.

(L) Quantification of c-Fos positive cells in paraventricular hypothalamic nucleus (n = 5-7, biological replicates). Data were analyzed by one-way ANOVA with Bonferroni multiple comparison test.

All data are reported as individual values or mean ± SEM.

Brain region abbreviations can be found in methods section 'unbiased whole-brain c-FOS imaging'.

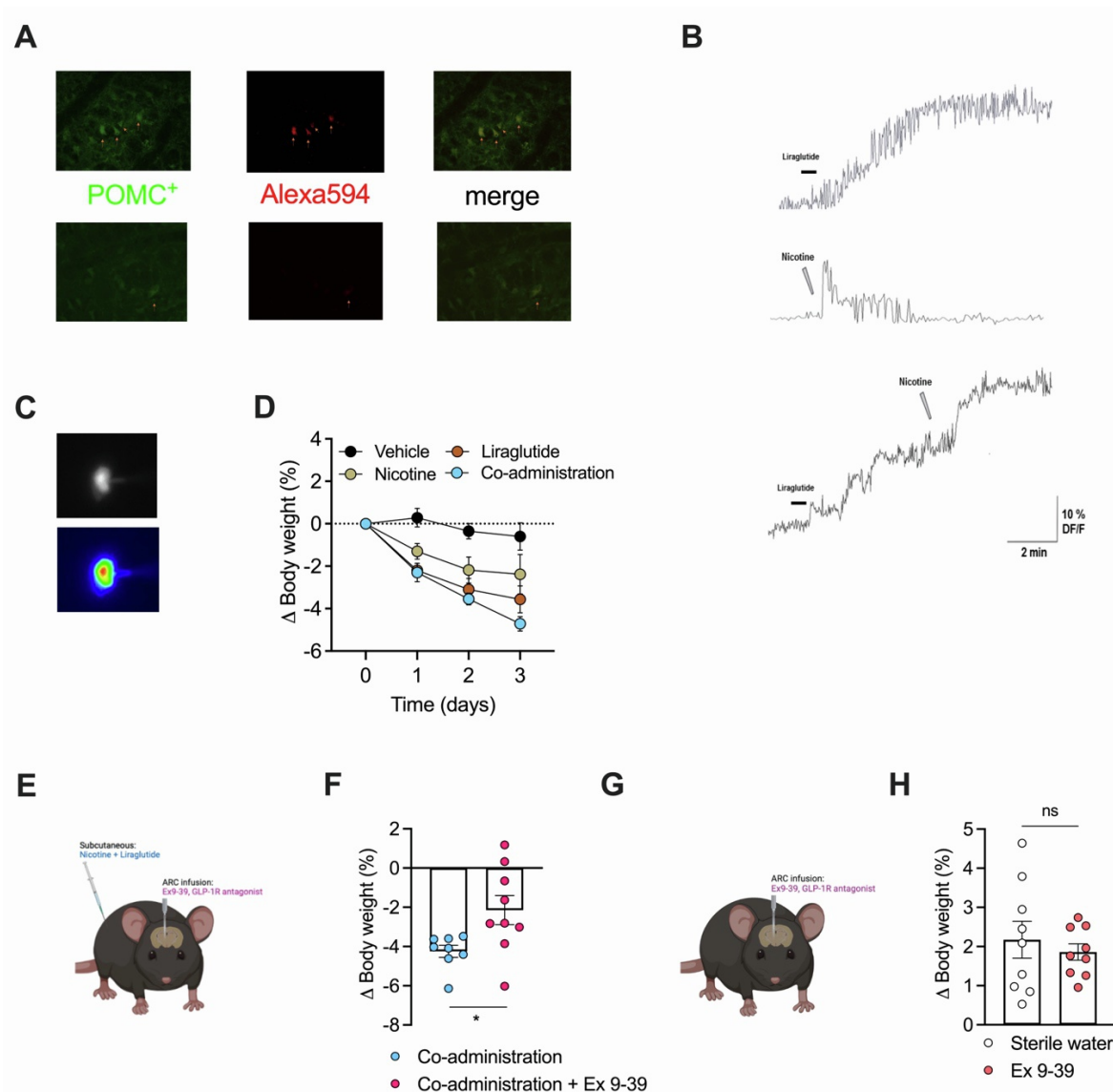


**Figure S3; Related to Figure 3. Effects of liraglutide and nicotine co-administration on the ARC.**

(A) Immunohistochemical validation of POMC<sup>+</sup> neurons in microdissected ARC brain slices used for the electrophysiology studies in Figure 3D-H.

(B) Representative traces from single-cell fluorescence calcium imaging of microdissected ARC brain slices in response to bath application of 100 nM liraglutide (upper), puff application of 10  $\mu$ M nicotine (middle) or combined bath application of 100 nM liraglutide and puff application of 10  $\mu$ M nicotine (lower).

(C) Representative pictures of fluorescence calcium imaging.

(D) Changes in body weight of mice in the RNA-sequencing study of ARC presented in Figure 3K-O (n = 5-6, biological replicates). Data were analyzed by two-way RM ANOVA with Bonferroni multiple comparison test.

(E) Illustration of study in high-fat diet (HFD)-induced obese C57BL/6J male mice receiving a single infusion of the GLP-1R antagonist Ex9-39 or sterile water into the ARC 30 minutes before s.c. injection of co-administration of liraglutide 10 nmol kg<sup>-1</sup> and nicotine 1 mg kg<sup>-1</sup>. Experiments were conducted using a cross-over design such that all mice received both treatments.

(F) Changes in body weight 24 hours after administration of experimental compounds (n = 8-9, biological replicates). One outlier was detected by Grubbs' test for Co-administration + sterile water infusion. Data were analyzed by a paired two-tailed t test, \*p < 0.05.

(G) Illustration of study in high-fat diet (HFD)-induced obese C57BL/6J male mice receiving a single infusion of the GLP-1R antagonist Ex9-39 or sterile water into the ARC. Experiments were conducted using a cross-over design such that all mice received both treatments.

(H) Changes in body weight 24 hours after administration of experimental compounds (n = 9, biological replicates). Data were analyzed by a paired two-tailed t test.

All data are reported as individual values or mean  $\pm$  SEM.

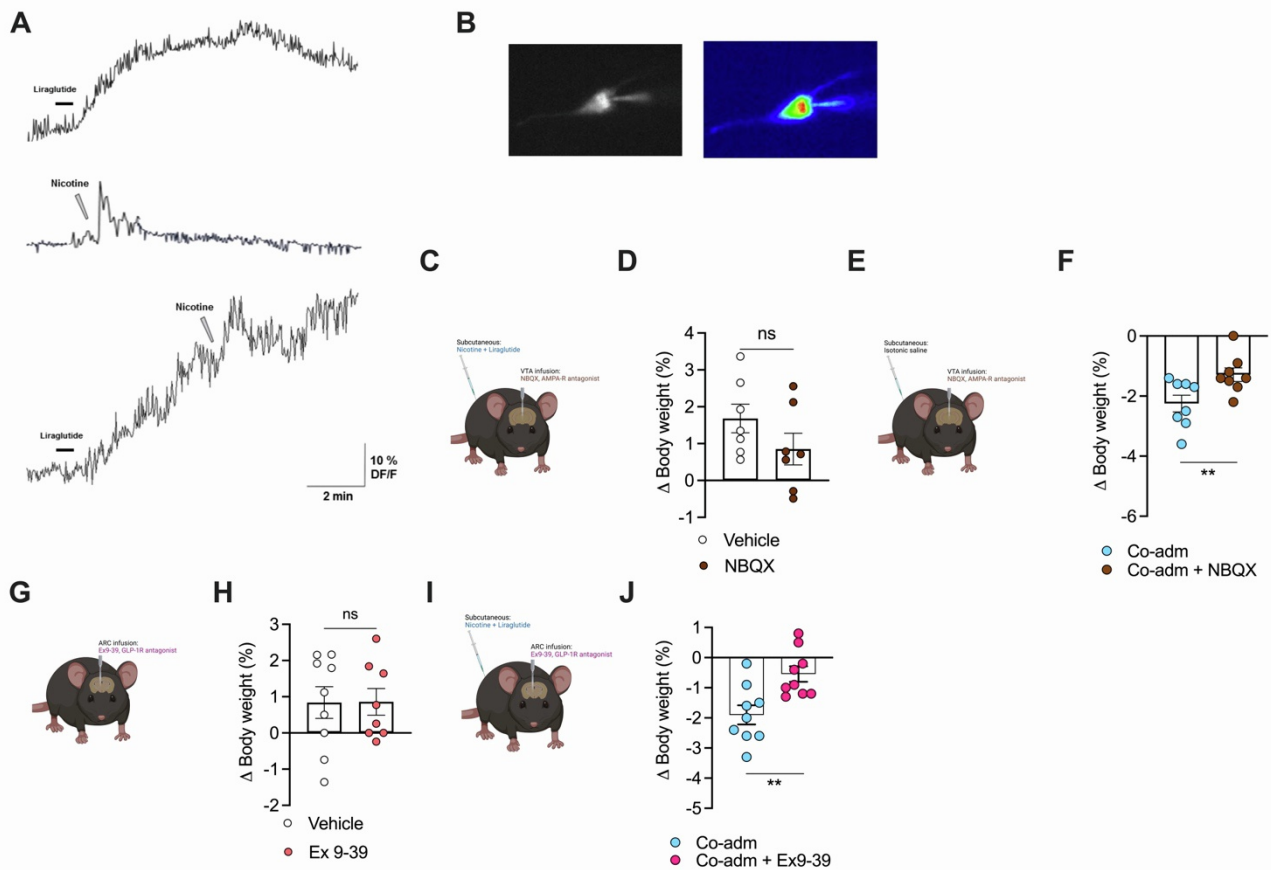


**Figure S4; Related to Figure 4. Effects of liraglutide and nicotine co-administration on the VTA.**

(A) Representative traces from single-cell fluorescence calcium imaging

(B) Representative traces from single-cell fluorescence calcium imaging of microdissected VTA brain slices in response to bath application of 100 nM liraglutide (upper), puff application of 10  $\mu$ M nicotine (middle) or combined bath application of 100 nM liraglutide and puff application of 10  $\mu$ M nicotine (lower).

(C) Illustration of study in high-fat diet-induced obese C57BL/6J male mice receiving a single infusion of the AMPA receptor antagonist NBQX or sterile water into the VTA. Experiments were conducted using a cross-over design such that all mice received both treatments.

(D) Changes in body weight 24 hours after administration of experimental compounds (n = 9, biological replicates). Data were analyzed by a paired two-tailed t test.

(E) Illustration of study in high-fat diet-induced obese C57BL/6J male mice receiving a single infusion of the AMPA receptor antagonist NBQX or sterile water into the VTA 30 minutes before s.c. injection of co-administration of liraglutide 10 nmol kg<sup>-1</sup> and nicotine 1 mg kg<sup>-1</sup>. Experiments were conducted using a cross-over design such that all mice received both treatments.

(F) Changes in body weight 24 hours after administration of experimental compounds (n = 9, biological replicates). One mouse was excluded due to sickness. Data were analyzed by a paired two-tailed t test, \*\*p < 0.01.

(G) Illustration of study in high-fat diet-induced obese C57BL/6J male mice receiving a single infusion of the GLP-1R antagonist Ex9-39 or sterile water into the VTA. Experiments were conducted using a cross-over design such that all mice received both treatments.

(H) Changes in body weight 24 hours after administration of experimental compounds (n = 9, biological replicates). Data were analyzed by a paired two-tailed t test.

(I) Illustration of study in high-fat diet-induced obese C57BL/6J male mice receiving a single infusion of the GLP-1R antagonist Ex9-39 or sterile water into the VTA 30 minutes before s.c. injection of co-administration of liraglutide 10 nmol kg<sup>-1</sup> and nicotine 1 mg kg<sup>-1</sup>. Experiments were conducted using a cross-over design such that all mice received both treatments.

(J) Changes in body weight 24 hours after administration of experimental compounds (n = 9, biological replicates). Data were analyzed by a paired two-tailed t test, \*p < 0.05.

All data are reported as individual values or mean  $\pm$  SEM.

**A**

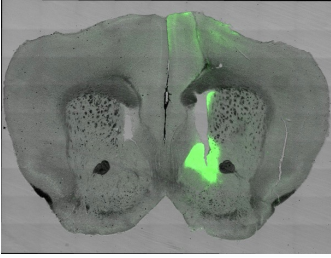


**Figure S5: Related to Figure 5. Fiber photometry recordings from the nucleus accumbens.**  
(A) Verification of fiber location and dLight1.3b expression enhanced with green-fluorescence protein.